J/ψ cross-section and event activities in p+p $\sqrt{s} = 200$ GeV at STAR

Bingchu Huang
bingchu@uic.edu

February 24, 2018

Contents

1 Introduction

Heavy flavor particle production in p+p collisions is an excellent tool of testing the perturbative Quantum Chromodynamics (pQCD) based models at RHIC. The J/ψ production in p+p collisions has been measured in various energies, however, it is still a challenge to understand the production mechanism due to the non-perturbative aspect of QCD e.g the evolution of the $c\bar{c}$ pair to the bound state. All the present models or production mechanisms discussed follow various approaches, mainly differing in the treatments of the hadronisation. The Color-Evaporation Model (CEM), the Color Singlet Model (CSM), and the Color Octet Model (COM), can reasonably describe the p_T dependent J/ψ measurements from RHIC and LHC within sizable uncertainties. The latter two are based on the effective Non-Relativistic Quantum Chromodynamics (NRQCD). However, current models are not able to consistently describe data in all experiments. Preciser measurements essentially help to understand of the J/ψ production mechanism, and constrain the models.

In addition to the p_T dependent cross section, the yields of the J/ψ is heavily sensitive to the particle production mechanisms and can help distinguishing between them. The bound states of c quark pairs in p+p collisions can be results from the Multiple-Partonic Interaction (MPI) with some higher order contributions from gluon splittings and radiations. In high multiplicity events, the MPI has substantial contributions on the particle production, which was treated as only affecting processes of light quarks and gluons before. However, recent studies at ALICE observed that a stronger-than-linear increment of the heavy flavor meson and quarkonia as a function of relative charged-particle multiplicity, which indicates that hard processes are also involved in the MPI. J/ψ production with respect to the charged-particle multiplicity can serves as a valuable probe on studying the particle production mechanism in p+p collisions, it can be interpreted in terms of the hadronic activity accompanying J/ψ production, as well as in terms of parton-parton interactions, or in the percolation scenario. Moreover, the treatment of the MPI is different in different models and event generators, therefore, the measurement of J/ψ in different multiplicity events can further constrain the models and generators that widely used in the high energy physics, such as PYTHIA and EPOS,

Table 1: Selected data sets in p+p at 200 GeV in run12.

Name	Trigger Ids	Luminosity (pb^{-1})	N_{events} (M)
BBCMB	370022	0.000	5.788
VPDMB-nobsmd	370011	0.029	734.853
BHT0*BBCMB*TOF0	370542	1.358	38.731
BHT1*BBCMB*TOF0	370546	9.422	40.821
BHT2*BBCMB	370522	23.513	35.977

2 Data set

Three data sets are used for J/ψ signal reconstructions. VPDMB-nobsmd data contain minimum bias events triggered by VPD detectors, the data are favorable for the reconstruction of low p_T J/ψ . There are three BEMC triggered data sets, BHT0, BHT1, and BHT2, with different thresholds of high towers. Results from BHT1 have large p_T overlap with the other two, and don't have significant improvement at the overlap p_T . Thus the BHT0 and BHT2 are selected for this analysis. Both BHT0 and BHT2 are combined with BBC east-west coincidence requirement, and one addition condition of TOF multiplicity (TOF0) is applied to BHT0 trigger in order to reduce pile-up events. Further more, BBCMB triggered events are suitable for calculating the unbiased TOF track multiplicity in MB. Table 1 shows the number of events and integrated luminosity for the data sets.

To reduce the pile-up events, a cut of vertex-z difference of 6 cm between vz measured by TPC and VPD is applied to the VPDMB-nobsmd. For other samples, there is no need for this cut as the samples are not triggered by the VPD. A cut on vertex z measured in TPC, $|vz| < 50$ cm, is applied for all the data sets. Ranking cut is not applied to any dataset to avoid bias on track multiplicity distributions. Table 2 shows the number of events after these cuts. Bad runs are studied in heavy flavor decayed electron analysis, following runs are rejected: 13041002, 13041010, 13042003, 13044118, 13045145, 13047004, 13047014, 13047044, 13047046, 13047050, 13048031, 13049052, 13052063, 13053021, 13054020, 13054057, 13057053, 13058047, 13058048, 13059079, 13060001, 13061024, 13061025, 13061026, 13064030, 13066101, 13066102, 13066104, 13066109, 13067001, 13068084, 13069068, 13070019, 13070030, 13070056, 13070057, 13070058, 13070059, 13070060, 13070061, 13071003, 13071004, 13071006, 13071006,

Table 2: Number of events after vz cuts.

Name	V_z Cuts	N_{events} after V_z cuts (M)
BBCMB	$\|v_z\| < 50\ cm$	2.66
VPDMB-nobsmd	$\|v_z\| < 50\ cm$, $\|\Delta V_z\| < 6\ cm$	306
BHT0*BBCMB*TOF0	$\|v_z\| < 50\ cm$	21.78
BHT1*BBCMB*TOF0	$\|v_z\| < 50\ cm$	22.52
BHT2*BBCMB	$\|v_z\| < 50\ cm$	20.77

13071008, 13071034, 13071037. The detail QA can be found at: `http://portal.nersc.gov/project/star/xiaozhi/Run_QA/RunQA_V4.pdf`

3 PYTHIA settings

In J/ψ cross-section and event activity studies, we frequently use the PYTHIA generators. Before we discuss the simulation details used in the analysis. We list all the versions and settings in this session for later references.

We use two versions of PYTHIA: 6.4.28 and 8.1.62 in PYTHIA + Geant simulation. The tunes for PYTHIA6 is as following:

Listing 1: PYTHIA6

```
pythia6->SetFrame("CMS", 200.0 );
pythia6->SetBlue("proton");
pythia6->SetYell("proton");
pythia6->PyTune( 320 );
//320 Perugia 0 Tuned by P. Skands, hep-ph/1005.3457
/*Physics Model: T. Sjostrand & P. Skands, hep-ph/0408302
          CR by P. Skands & D. Wicke, hep-ph/0703081
          LEP parameters tuned by Professor, hep-ph/0907.2973*/
```

We use two tunes of PYTHIA 8.1.62, which are STAR default settings and STAR heavy flavor tunes: STAR default settings are shown in Tab. 3:

Settings with " * " are for J/ψ simulations.

STAR heavy flavor tune is listed below:

In summary, there are 3 settings used in simulations: PYTHIA6.4.28 Perugia tune, PYTHIA8.162 STAR default tune, and STAR heavy flavor tune.

Table 3: STAR PYTHIA default settings.

Name	Now	Default	Min	Max
BeamRemnants:reconnectRange	1.5	10.0	0.0	10.0
Beams:eCM	200.0	14000.	10.0	/
* HardQCD:all	on	off	/	/
* HardQCD:gg2ccbar	on	off	/	/
* HardQCD:qqbar2ccbar	on	off	/	/
MultipartonInteractions:alphaSvalue	0.135	0.127	0.06	0.25
MultipartonInteractions:bProfile	3	1	0	4
MultipartonInteractions:ecmPow	0.19	0.24000	0.0	0.50
MultipartonInteractions:expPow	2.0	1.00000	0.40	10.0
MultipartonInteractions:pT0Ref	2.085	2.15000	0.50	10.0
PhaseSpace:pTHatMax	128.0	-1.00000	/	/
SigmaDiffractive:dampen	on	off	/	/
SigmaDiffractive:maxAX	65.0	15.0000	0.0	/
SigmaDiffractive:maxXB	65.0	15.00000	0.0	/
SigmaDiffractive:maxXX	65.0	15.00000	0.0	/
SigmaProcess:alphaSvalue	0.135	0.12650	0.06	0.25
SpaceShower:rapidityOrder	on	off	/	/
StringFlav:mesonCvector	1.5	1.06000	0.0	3.0

Table 4: STAR PYTHIA HF tune settings.

Name	Now	Default	Min	Max
Beams:eCM	200.0	14000.000	10.00000	
* HardQCD:all	on	off		
ParticleDecays:limitCylinder	on	off		
ParticleDecays:xyMax	600.0	10.00000	0.0	
ParticleDecays:zMax	1000.0	10.00000	0.0	
PDF:extrapolateLHAPDF	on	off		
PDF:LHAPDFset	MRSTMCal	MRST2004FF4lo		
PDF:useLHAPDF	on	off		
PhaseSpace:pTHatMax	1.0	-1.00000		
Random:seed	767	-1	900000000	
Random:setSeed	on	off		
SigmaProcess:factorMultFac	2.0	1.00000	0.10000	10.00000
SigmaProcess:factorScale2	3	1	1	5
SigmaProcess:renormMultFac	2.0	1.00000	0.10000	10.00000
SigmaProcess:renormScale2	3	2	1	5
StringFlav:mesonCvector	1.5	1.06000	0.0	3.00000

4 Track selection

Basic track quality cuts are summarized in Table. 5. To select electron candidates, three detectors are used in the analysis: TPC, TOF, and BEMC. Normalized dE/dx, nσ_e , measured by TPC is used to reduce hadrons. $1/\beta$ from TOF is used to remove slow hadrons at low p_T . p/E from BEMC further reduce hadrons at high p_T . In addition to $1/\beta$, a cut of local Y position relative to TOF sensor center is applied to remove bad matched tracks. These cuts are shown in Table. 6. Two combinations are used to select electron candidates, TPC+TOF and TPC+BEMC. In the following text, we will use "TOF electron" and "BEMC electron" to note these two combinations, respectively. Figure 1 shows the TOF $1/\beta$ vs p distribution. Figure 2 shows the p/E vs p of photonic electrons. Figure 3 shows the nσ_e distributions after different eID cuts. We can see that the eID cuts capture the electron candidates quite well.

For BEMC high tower (HT) triggered events, different online thresholds are used to select tracks in different kinetic ranges. Three thresholds 11

Table 5: Track quality cuts.

$0.2 < p_T < 50$ GeV/c
$-1 < \eta < 1$
$dca < 1\ cm$
$nHitsFit >= 20$
$nHitsdEdx >= 11$
$nHitsRatio > 0.52$

Table 6: Particle identification (PID) cuts.

Type	Cuts
TPC electrons	$-1.9 < n\sigma_e < 3$
TOF electrons	$\lvert localY\rvert < 2\ cm$
	$\lvert 1/\beta - 1\rvert < 0.03$
BEMC electrons	$p_T > 1$ GeV/c
	$0.3 < p/E < 1.5$

(HT0), 15 (HT1), and 18 (HT2) are applied on the online DSM recorded ADC value to trigger events, more specific DSMADC > 11, 15, and 18. The corresponding offline ADC0 are required larger than 180, 250, and 300 for HT0, HT1, and HT2, respectively. HT1 data have large overlap with HT0 and HT2, therefore, HT1 data are not used in the analysis. There are hot towers in HT triggered events, they have been studied in NPE analysis. In this analysis, following towers are marked as hot towers and not used in the analysis: 31, 51, 114, 275, 293, 479, 509, 533, 555, 561, 639, 681, 740, 743, 749, 772, 779, 799, 840, 860, 880, 893, 897, 982, 986, 993, 1063, 1142, 1160, 1200, 1224, 1232, 1237, 1241, 1256, 1263, 1280, 1284, 1306, 1313, 1318, 1337, 1438, 1486, 1537, 1592, 1709, 1713, 1732, 1823, 1850, 1856, 1879, 1945, 1976, 1984, 2043, 2145, 2162, 2164, 2190, 2202, 2290, 2299, 2300, 2313, 2339, 2414, 2439, 2459, 2529, 2580, 2633, 2652, 2834, 2863, 2865, 2874, 3005, 3020, 3061, 3137, 3154, 3420, 3515, 3532, 3692, 3720, 3737, 3838, 3861, 3925, 3948, 4013, 4130, 4169, 4262, 4316, 4430, 4458, 4534, 4560, 4595, 4684, 4766, 4781. In later efficiency study, these towers are rejected as well.

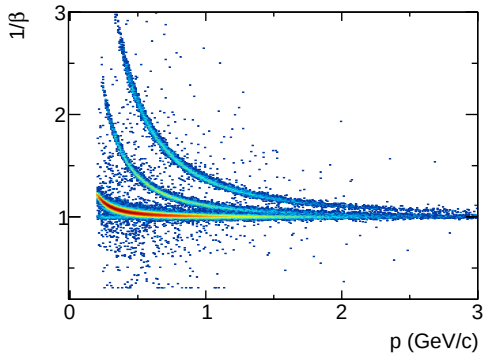

Figure 1: $1/\beta$ vs. momentum distribution.

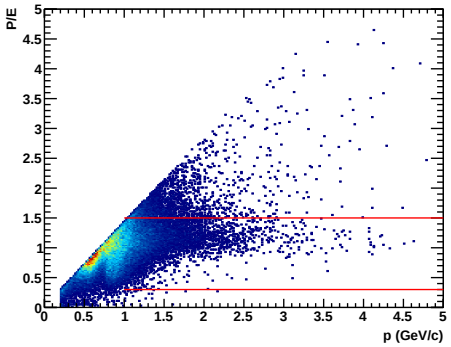

Figure 2: photonic electron p/E vs. momentum distribution.

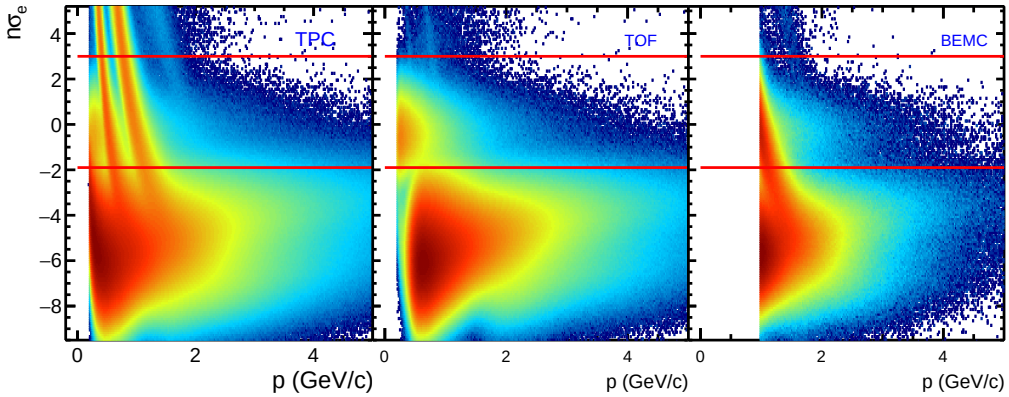

Figure 3: $n\sigma_e$ for TPC tracks with no cuts (left), TOF eID cuts (middle), and BEMC eID cuts (right).

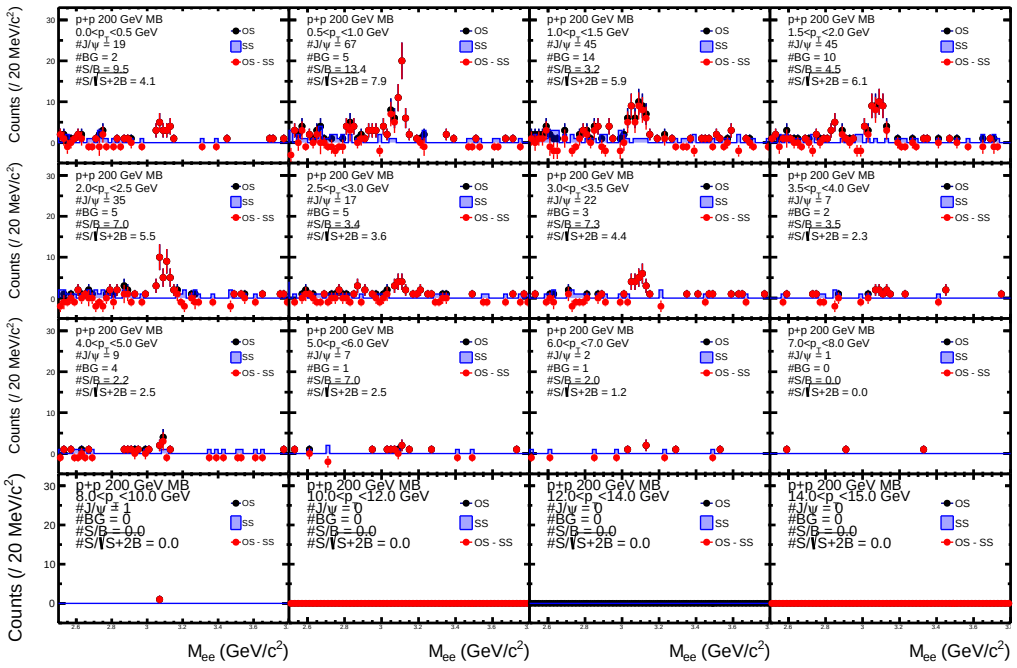

Figure 4: ee pair invariant mass in different p_T bins from MB events.

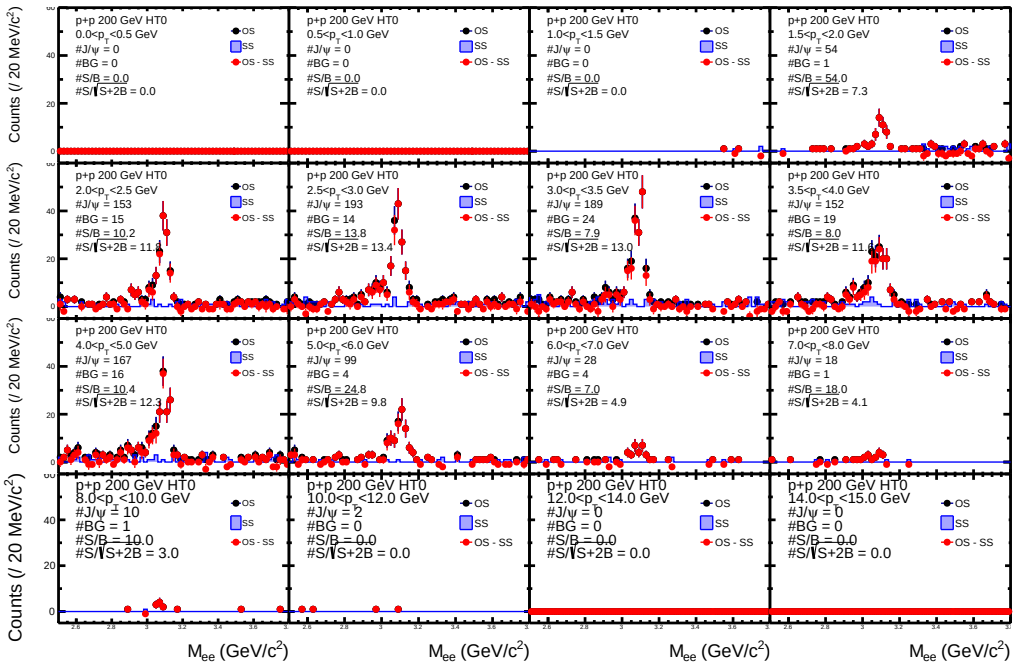

Figure 5: ee pair invariant mass in different p_T bins from HT0 events.

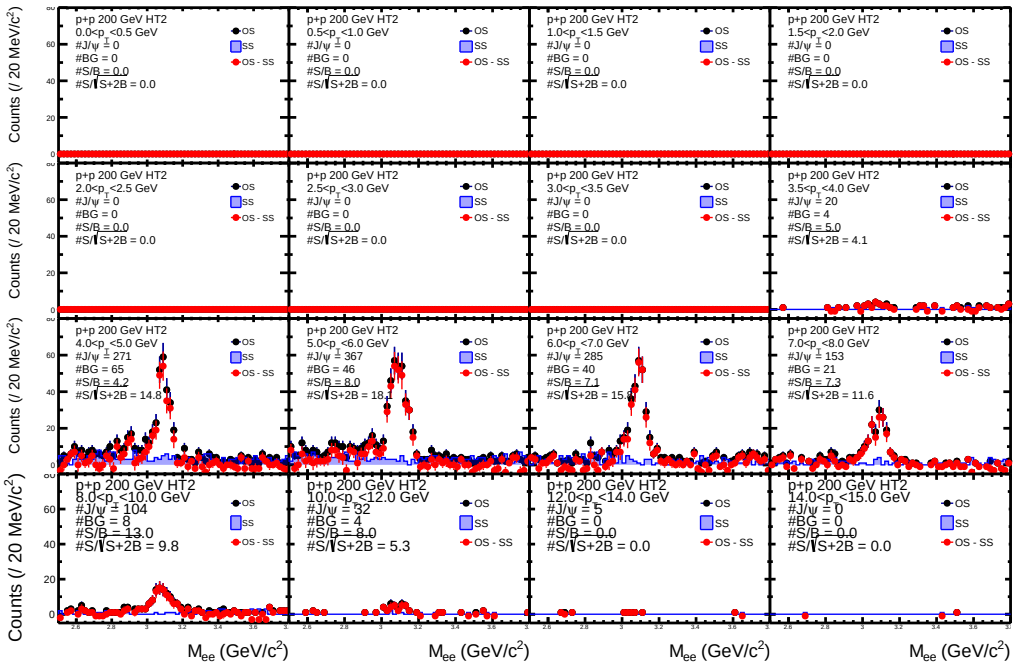

Figure 6: ee pair invariant mass in different p_T bins from HT2 events.

5 J/ψ yield extraction

5.1 J/ψ raw signals

J/ψ signals are reconstructed by pairing two electrons in same event that both pass at least one eID cut. In MB data sample, both electrons in a pair must be either TOF or EMC electron. For HT events, at least one track has to satisfy both BEMC eID and trigger requirement (ADC0 ¿ threshold as mentioned in last section), another track can be either TOF or EMC electron. The pair rapidity is required to be within (-1,1). Figure 4, Figure 5, and Figure 6 show the invariant mass spectra of electron pairs for MB, HT0, and HT2 events, respectively. Three data samples cover full p_T range 0-14 GeV/c. Here the number of J/ψ counts is from counts in (2.9,3.2) GeV/c^2 .

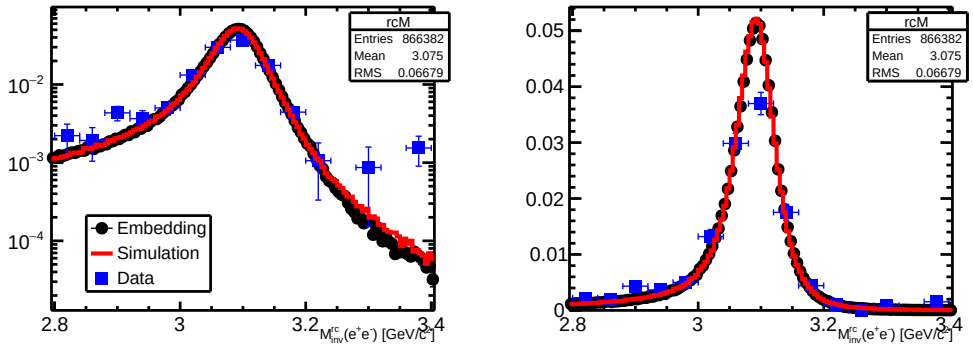

Figure 7: J/ψ mass from data, embedding, and simulation without tuning. Left is log scale.

5.2 J/ψ raw signal fit

J/ψ raw signals are fitted by mass distributions from a Toy Monte-Carlo with a tuned momentum resolution. The procedure is as following:

1 Fill the $(p_T^{MC} - p_T^{RC})/p_T$ vs p_T distribution from embedding, from which $\sigma(\Delta p_T/p_T)$ as a function of p_T is obtained.

2 Fit the $\sigma(\Delta p_T/p_T)$ as a function of p_T using function $f(p_T) = \sqrt{a^2 p_T^2 + b^2}$.

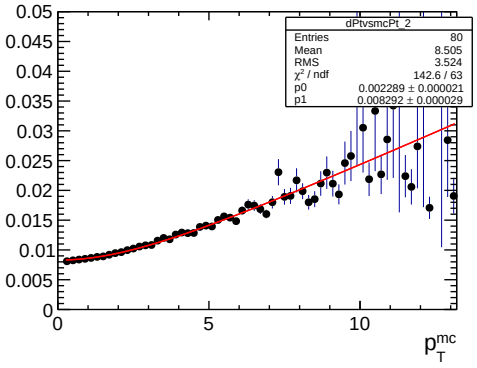

Figure 8: Momentum resolution $\sigma(\Delta p_T/p_T)$ as a function of p_T, fit with a function of $f(p_T) = \sqrt{a^2 p_T^2 + b^2}$.

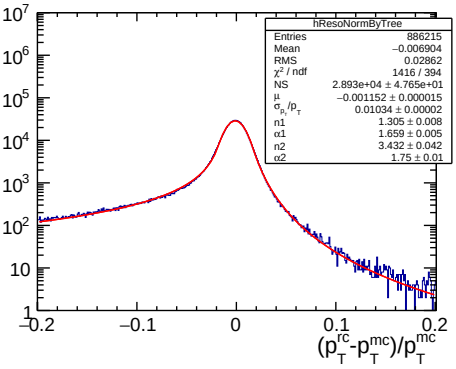

Figure 9: Double Crystal Ball function fit to the normalized $\Delta p_T\ /p_T$.

3 Fill the $(p_T^{MC} - p_T^{RC})/p_T$ vs p_T distribution again after dividing $(p_T^{MC} - p_T^{RC})/p_T$ by the $\sigma(\Delta p_T/p_T)$ obtained in previous step and multiplying by 0.01.

4 Fit the scaled $\Delta p_T/p_T$ distribution by a double crystal ball (DCB) function.

5 Tune the parameter a in step 2, sample the DCB function and the tuned width to obtained smeared momentum. Then calculate the χ^2 between the J/ψ mass distributions from data and simulation and find the best parameter lead to the minimum χ^2.

In our simulation, the p_T of two daughter electrons of J/ψ are smeared by DCB function multiply a p_T dependent σ, which is calculated by the resolution function with the parameters a and b. Figure 7 shows the result from our smear process in red line, which exactly reproduce the J/ψ mass shape from embedding. This process is done for each p_T bin. χ^2 calculation range is from 2.7 to 3.4 GeV/c^2 .

For last step, we scan a range to find the best a, the χ^2 of J/ψ mass distributions in simulation and data is calculated once a test parameter a is given. The minimum χ^2 is chosen to determine the parameters, which is shown in Fig. 10. The mass distributions of J/ψ are obtained in this simulation, and used to fit the raw signals. An 1st-order polynomial function

is added in the fit to represent residual background from $cc \to ee$. Figure 11 and Figure 12 show the fit results for three data samples. The maximum likelihood method is used in the fit. The raw counts are calculated by two methods, fit and bin counting. Bin counting method counts the signal within (2.9, 3.2) GeV/c^2 , and corrected for the mass-cut efficiency. The mass shape is from tuned embedding. The mass-cut efficiency decreases from 93% to 82% as J/ψ p_T increases. Fit method obtains the counts from the tuned J/ψ shape integral, which are used as central values. Result from bin counting method is accounted for systematic uncertainty. Results in p_T ranges 0-1.5, 1.5-4, and 4-14 GeV/c are chosen for MB, HT0, and HT2 results, respectively, they are combined into final result.

In addition, the statistical distribution of unlike-sign subtracted like-sign is neither Poisson nor Gaussian distribution. Both likelihood and least squares methods may have bias in low statistics bins. We compared the fitting results from two methods and bin counting, the difference between them are within statistical fluctuation. Given Likelihood method has better performance at lower statistical bin, it is used for central values. The difference of statistical errors between Likelihood and bin counting is negligible, thus the statistical errors are chosen from Likelihood. The comparison of three methods is shown in Fig. 13.

J/ψ may decay into lepton pair and photon thus form a long tail on the left hand side of the J/ψ mass shape. This effect has been studied in PSN0557, which adds 4-9% uncertainty to the raw yield. The variation of the mass window and background shape in fit covers this uncertainty, it will be discussed later.

5.3 Efficiency

There are several efficiencies need to be corrected for raw spectra: TOF matching, TPC tracking, $1/\beta$ cut, nσ_e cut, BEMC matching, p/E cut, and trigger efficiency. TOF matching, $1/\beta$, and nσ_e selection efficiencies are estimated in a data-driven way.

TPC and BEMC efficiencies can be well described by the embedding simulation. In the embedding sample, the MC tracks are embedded into real events and reconstructed by same procedures as real data production. Figure 14 and 15 show the comparisons of nHitsFit and nHitsDedx between tracks with $|n\sigma_e| < 2$ in data and reconstructed electrons in embedding sample, respectively. Figure 16 and 18 are the comparisons of p/E and

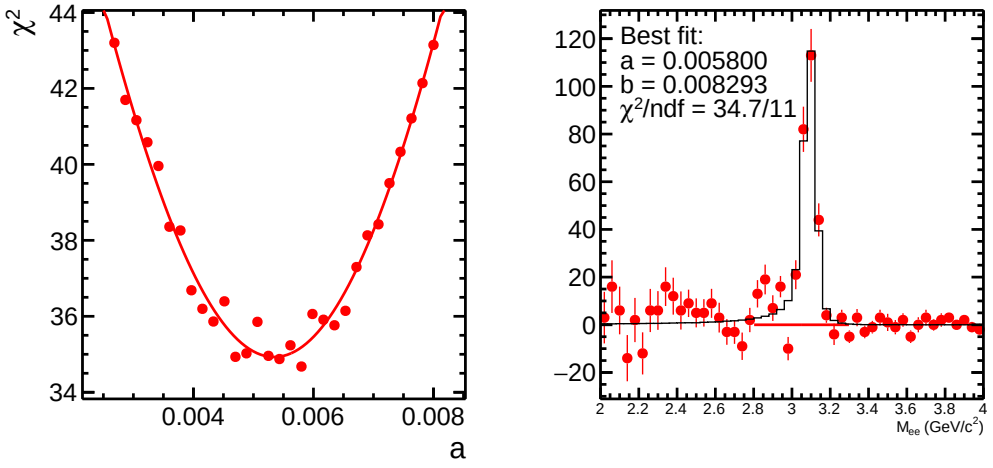

Figure 10: Best fit of J/ψ mass shape.

ADC0 using triggered electrons. The EMC matching is defined as the ratio of EMC matched tracks over TPC tracks after track quality cuts. For a cross check, Fig. 17 shows the EMC matching efficiency obtained from data and embedding obtained from run14 Au+Au 60-80%. It shows there is a difference at $p_T < 1$ GeV/c where we cut on EMC tracks. The minimum EMC track p_T requirement is varied by 0.1 GeV/c to estimate the uncertainty of the matching efficiency.

TPC tracks are selected from data with basic track quality cuts. Then TOF matching requirements ($\beta > 0$ and $|localY| < 2$ cm) are added on top of the TPC track selections to form another track set. The ratio between numbers of these two track sets is defined as TOF matching efficiency. It's hard to obtain clean electron sample in data without any eID cuts, therefore, two methods are used to estimate the TOF matching efficiency. First method selects tracks satisfying $|n\sigma_e| < 1$ and $|n\sigma_h| > 2$, h can be π, K, and proton. Since there are pile-up tracks in the data, we require tracks have EMC matching to reduce the pile-up in this method, which means there is a EMC hit associated with the track. Second method selects photonic electrons reconstructed from TPC tracks, which can form an ee pair with another TPC track passing several cuts, including opening angle $< \pi/10$, dca between two electrons < 1 cm, pair decay length > 5 cm, and pair mass < 0.05 GeV/c^2 . First method has more statistics, however, there are still some contamination

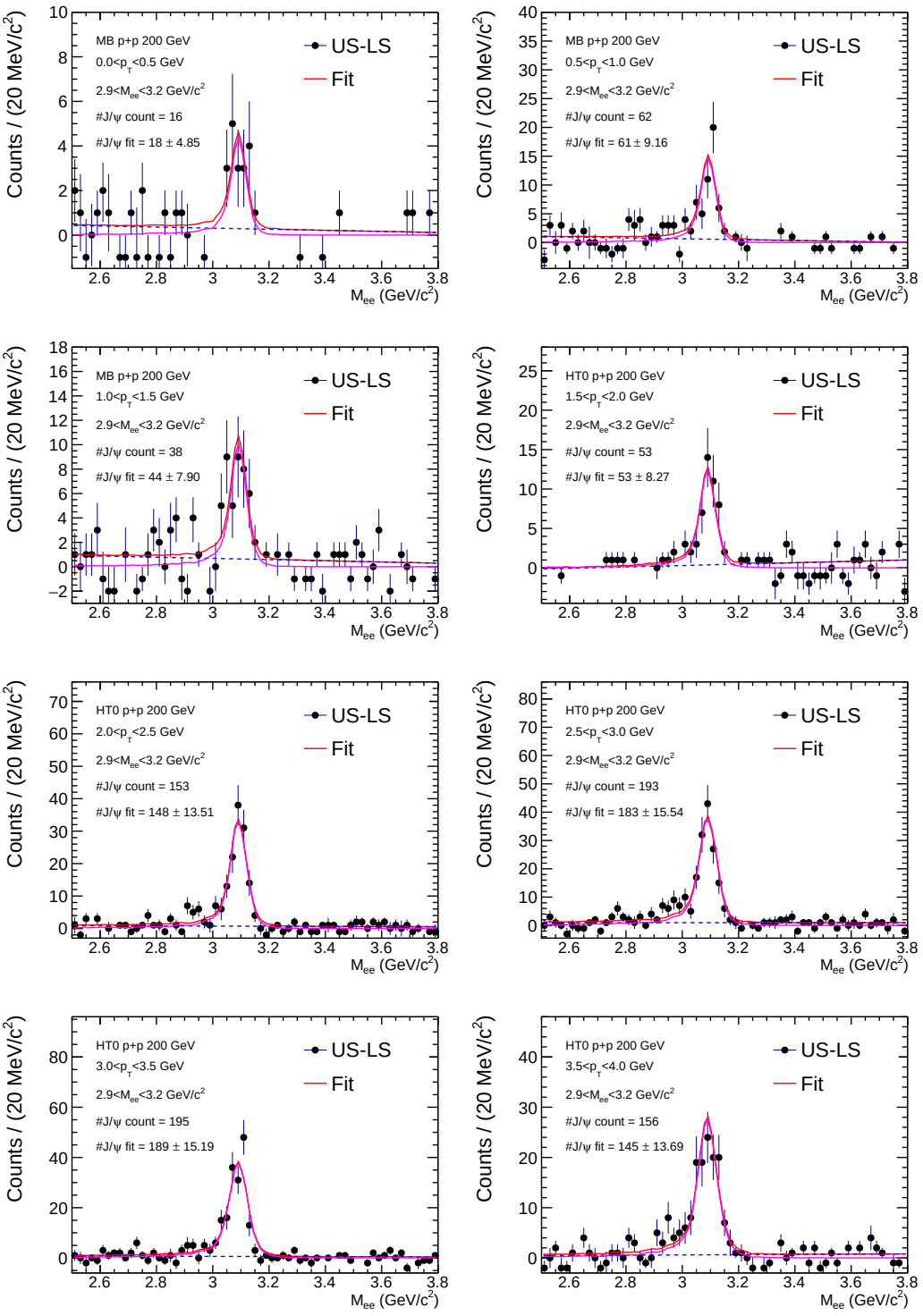

Figure 11: J/ψ signal fits. Dashed blue line is the exponential function representing residual background.

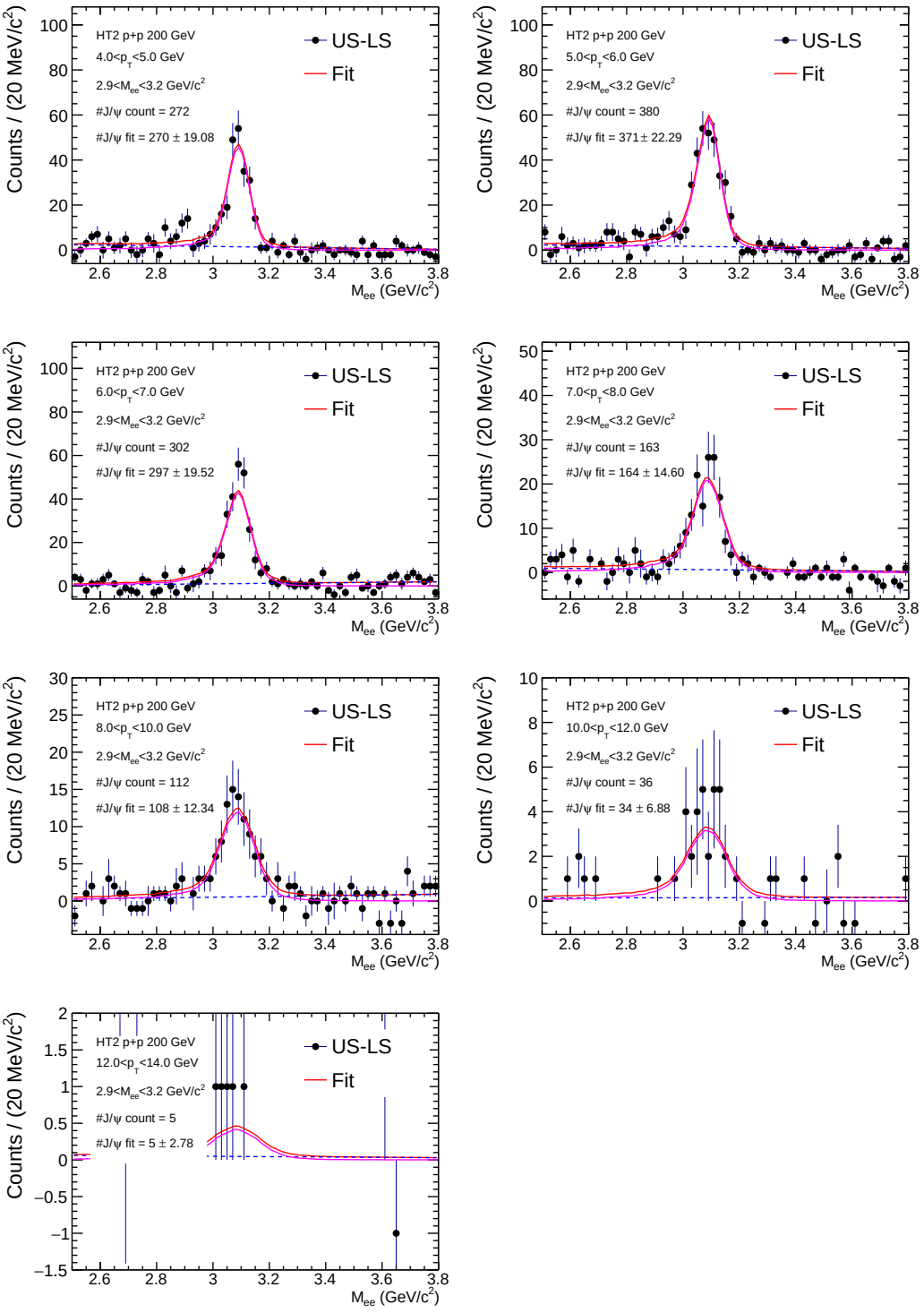

Figure 12: J/ψ signal fits.

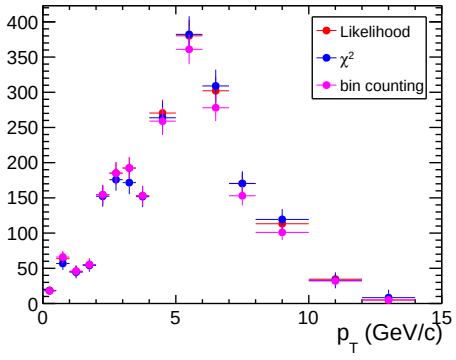

Figure 13: The comparison of three methods in J/ψ raw signal extraction.

from hadrons at dE/dx overlapping p_T range. Second method has much pure electrons, but lack of statistics. Since the p_T of electrons from J/ψ is usually greater than 1 GeV/c , the difference caused by hadron contamination at $p_T < 1$ GeV/c has very small effect on final results. Thus two methods are consistent with each other.

Figure 19 shows the overall TOF matching efficiency obtained from two methods, the momentum is primary momentum calculated with primary vertex as first point. Figure 20 and 21 show the efficiency in η range (-1,1) from first method of $|n\sigma_e| < 1$. Then TOF efficiency is calculated in 20 η bins, and fitted by a function $p_0 e^{-(p_1 * p_T)^{p_2}}$. The fit parameters are used later in J/ψ total efficiency calculation. The errors on parameters are used to vary the fit function to estimate the systematic uncertainties in 68% confidence level.

$1/\beta$ distribution of photonic electron is fitted by Gaussian function for each p_T slices. The mean and σ are shown in Fig. 23, they are used in J/ψ efficiency calculation. A constant function is fitted to measured mean and σ, then used in the efficiency calculation. x-axis is global p_T . Fit mean is 0.998 $\pm$ 2e-5 for mean, and fit σ is 0.012 $\pm$ 9.5e-5.

nσ_e distribution of photonic electron is also fitted by Gaussian function for each p_T slices. The mean and σ are nearly flat, they are fitted with a constant function, and parameters are used for later usage. The mean is -0.395 $\pm$ 0.0066, and σ is 0.871 $\pm$ 0.0051.

In pairing procedure, we select EMC electrons first, then seek for another candidate from TOF matching. In this way, the TOF efficiency has a dependence on EMC matching efficiency. On top of the J/ψ efficiency previously

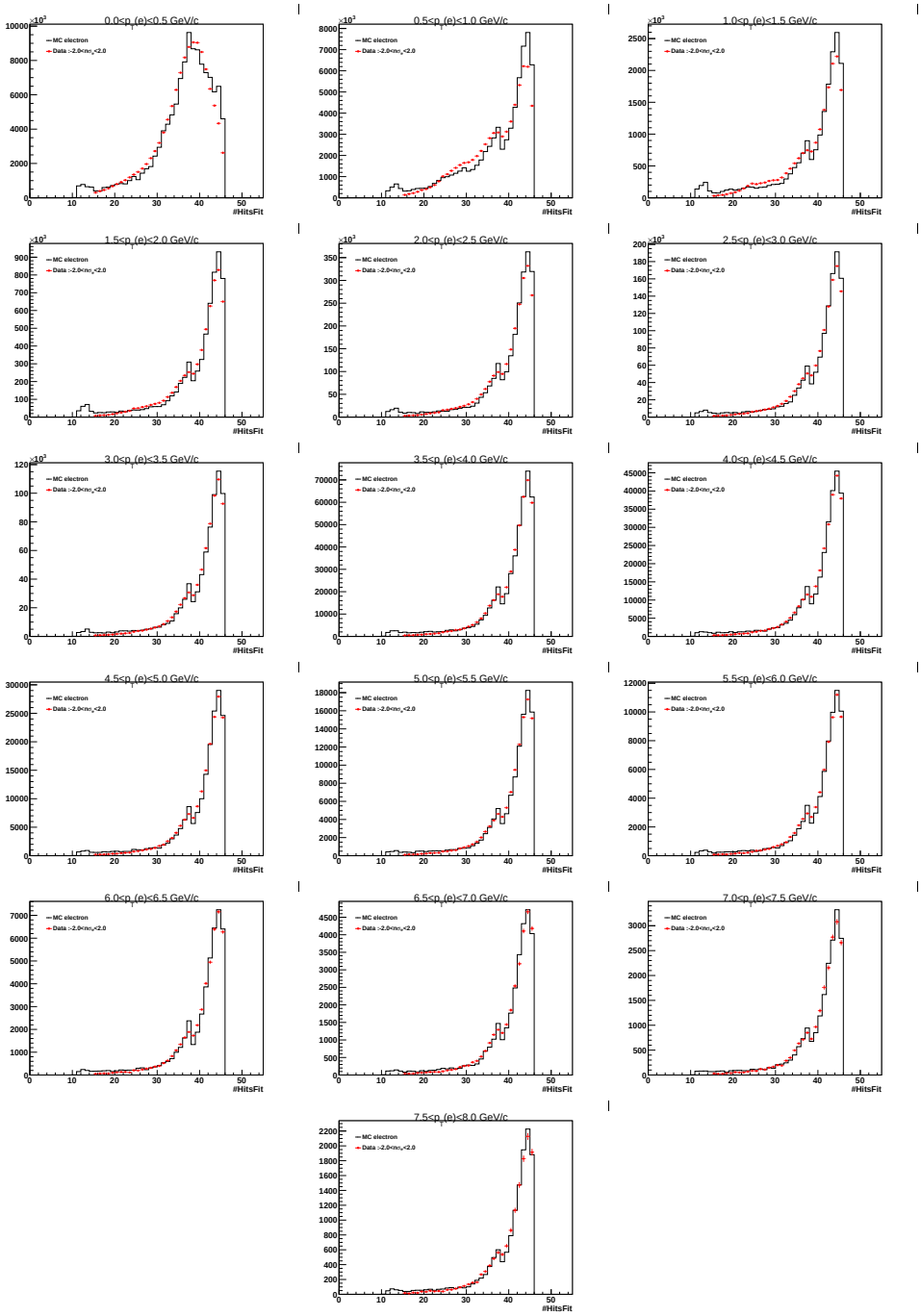

Figure 14: nHitsFit of electron in data and embedding.

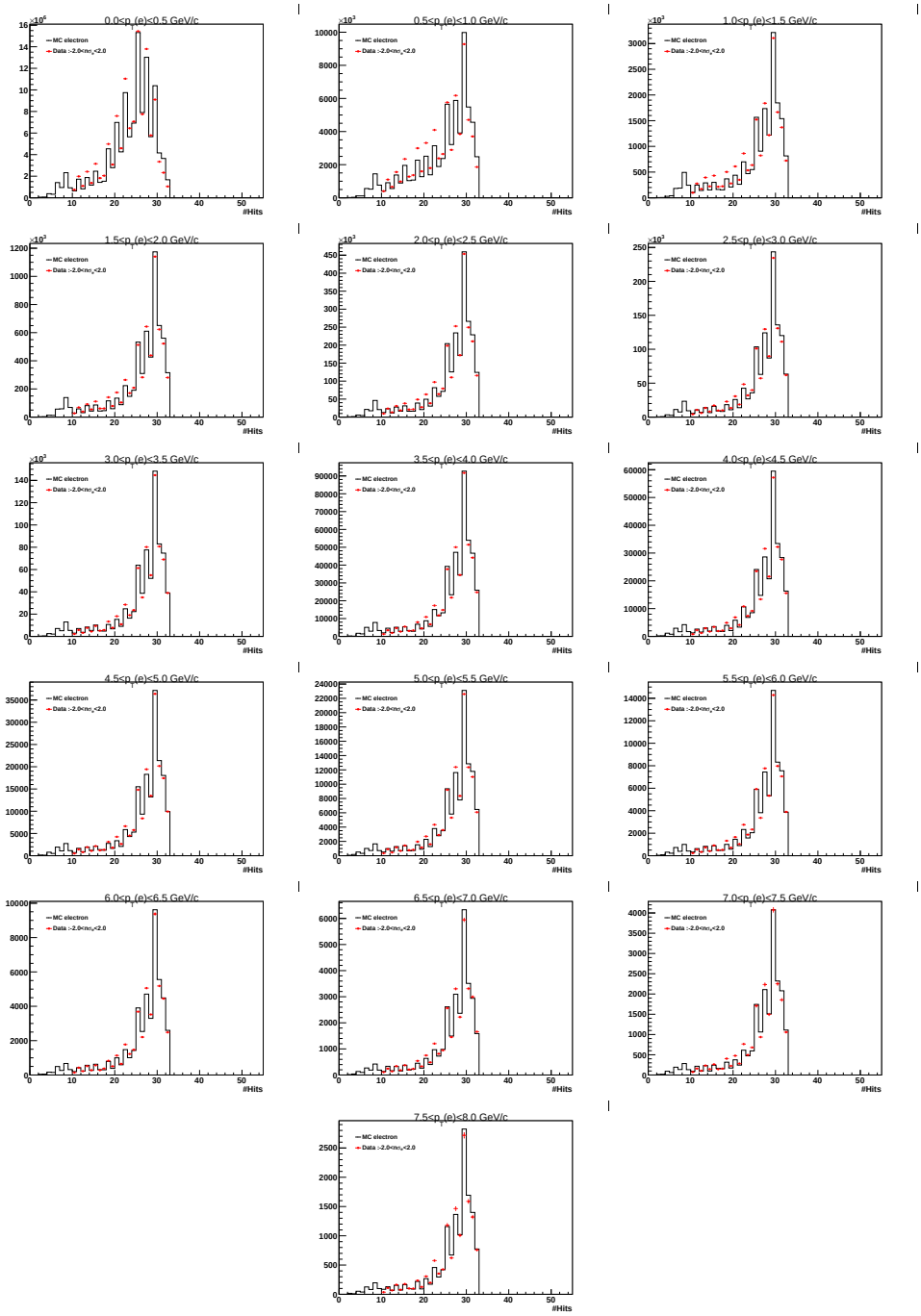

Figure 15: nHitsDedx of electron in data and embedding.

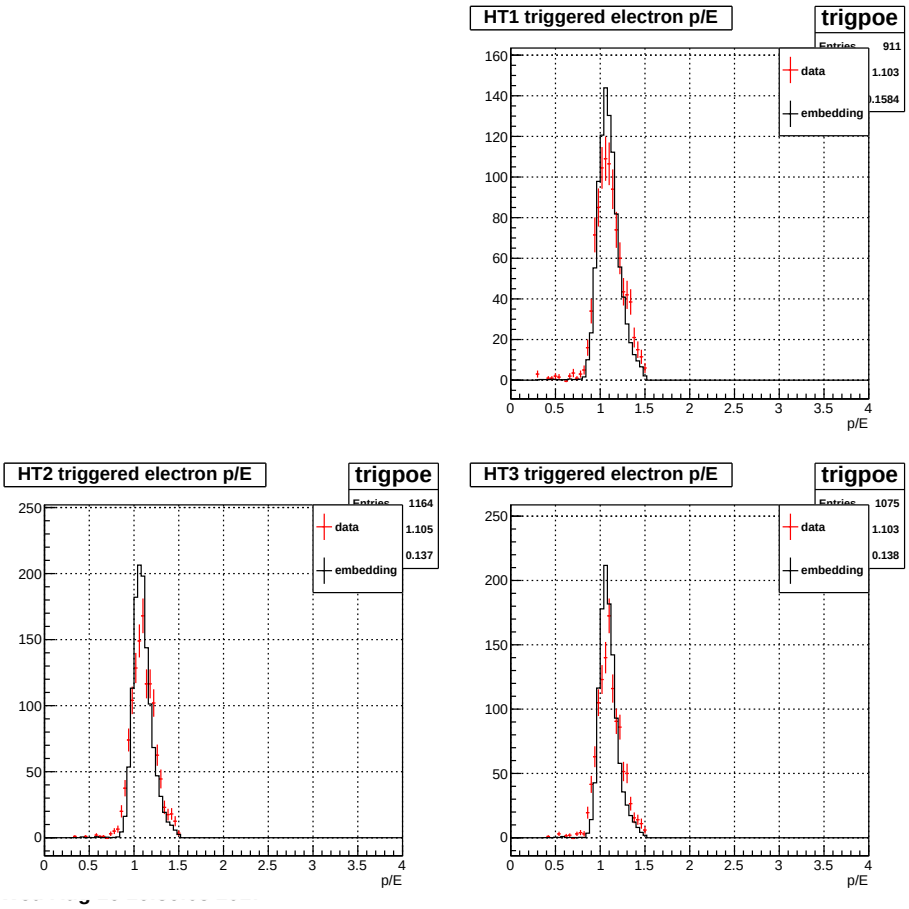

Figure 16: p/E comparison between data and embedding.

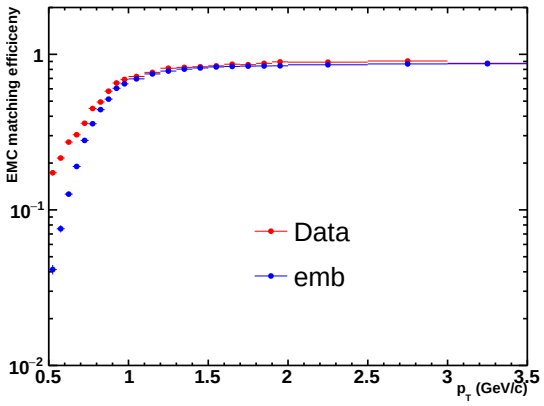

Figure 17: EMC matching efficiency comparison between data and embedding.

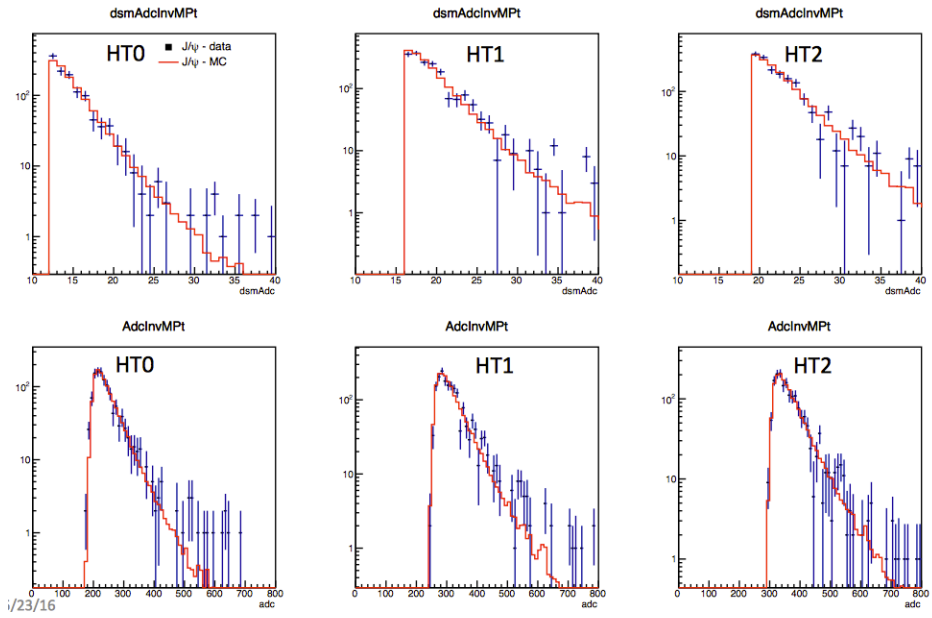

Figure 18: ADC and DSMADC comparison between data and embedding. Embedding is weighted by measured J/ψ p_T spectrum.

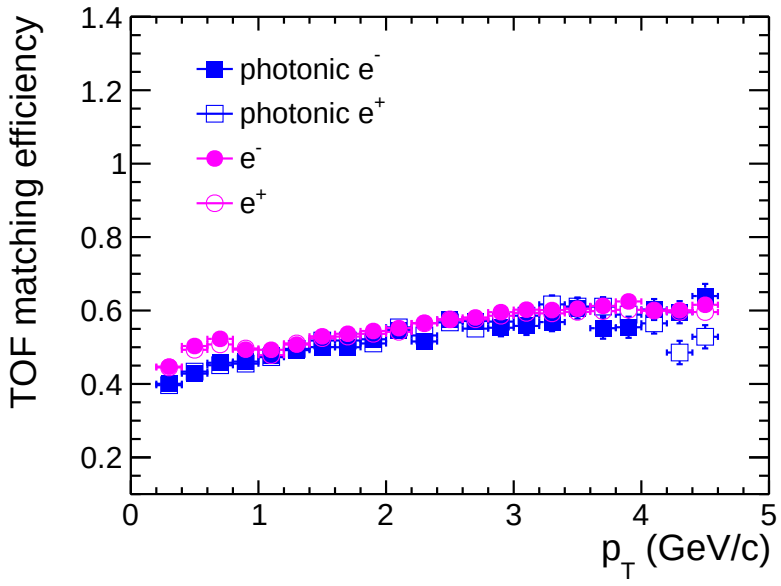

Figure 19: TOF matching efficiency calculated by two methods. Details are in text.

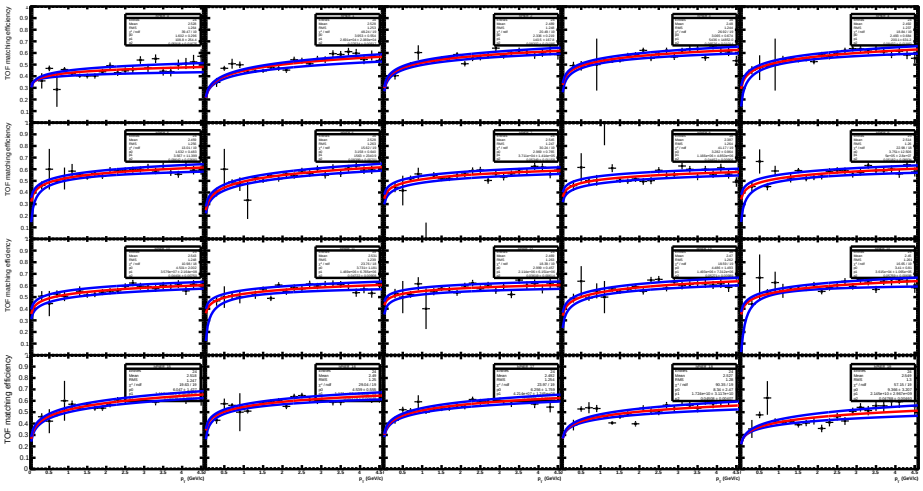

Figure 20: TOF matching efficiency of positron in η range (-1,1).

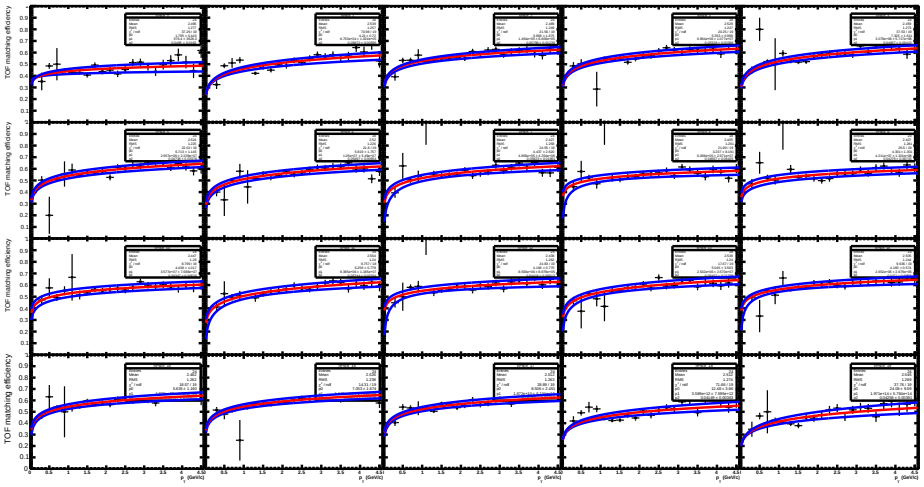

Figure 21: TOF matching efficiency of electron in η range (-1,1).

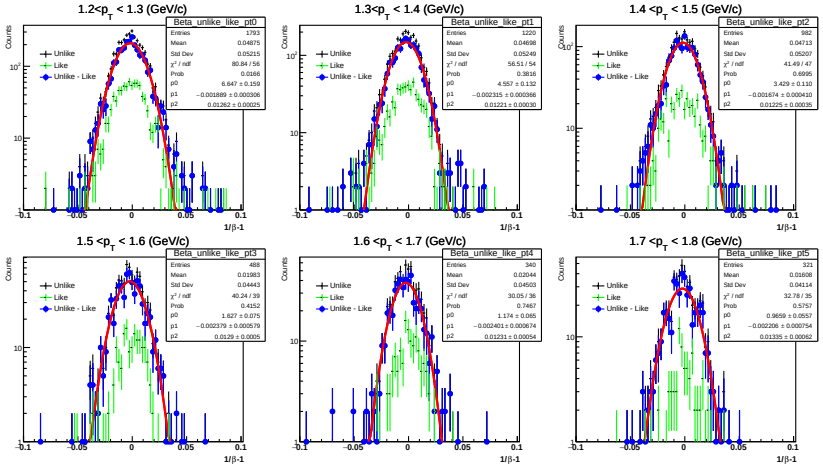

Figure 22: TOF $1/\beta$ fit for photonic electrons.

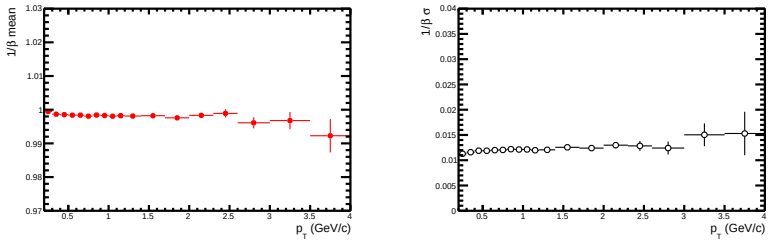

Figure 23: TOF $1/\beta$ mean and σ from photonic electrons.

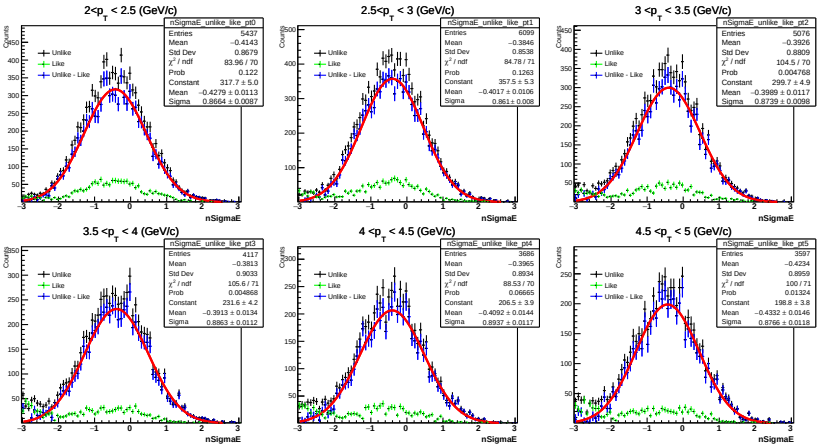

Figure 24: $n\sigma_e$ fit for photonic electrons.

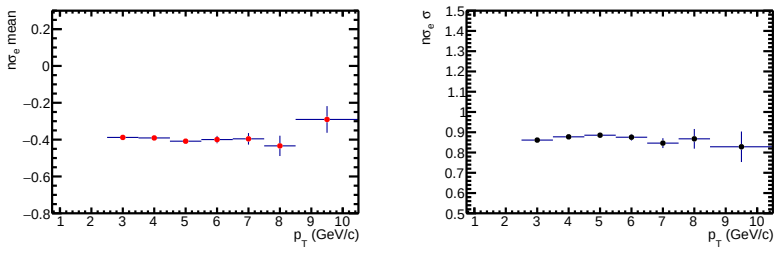

Figure 25: $n\sigma_e$ mean and σ from photonic electrons.

calculated, we need to calculate the TOF efficiency condition on no EMC matching. The following formula describe how we obtain this efficiency.

$$P(TOF) = P(TOF|EMC)P(EMC) + P(TOF|noEMC)P(noEMC) \quad (1)$$

$$P(TOF|noEMC) = \frac{P(TOF)(1 - P(EMC)/r)}{P(noEMC)} \quad (2)$$

where $r = P(TOF)/P(TOF|EMC)$ calculated from HT sample. Figure 26 shows this ratio of electron from this study and the ratio of pion from low luminosity runs used in 2011 D^* analysis (`http://www.star.bnl.gov/protected/heavy/tlusty/Dstar2011/PaperProposal/documents/note.pdf`). Since they are consistent and the ratio from low luminosity run is more precise. We use the pion r in Fig. 26 from low luminosity to calculate the TOF efficiency condition on no EMC matching. The correlation between TOF and EMC efficiencies depends on their geometrical acceptances. At high p_T, where the tracks are closer to straight lines, we expect the correlation independent of p_T, as Fig. 26 shows. Therefore, a constant extrapolation for the ratio r is applied to $p_T > 1$ GeV/c . With such an extrapolation the uncertainty at high p_T is determined by the low p_T uncertainty, which is negligible shown in the figure. We use the ratio r of electrons in Fig. 26 to calculate the J/ψ efficiency, and assign the difference between this efficiency and the one calculated by the r from pions as a uncertainty. The uncertainty is shown in Fig. 27.

Till now, all the data-driven efficiencies are ready to use in J/ψ total efficiency calculation. The embedding sample provides the kinetic and detector information of input J/ψ and its daughter electrons. To fold these data-driven efficiencies into reconstructed electrons, a random generator is used to simulate the survival rates of individual requirements. For an electron with a certain p_T , the TOF matching, $1/\beta$, and nσ_e efficiencies are calculated by the fit functions mentioned earlier. If the random generator gives a random number within (0,1), which is less than the efficiency value, then this track is kept in J/ψ reconstruction. Other cuts are applied for the track in same way as the data analysis. In this way, the reconstructed J/ψ in embedding passes through all the cuts used in the data analysis. In the embedding sample, the input J/ψ has a flat p_T and rapidity distribution. To calculate the real efficiency, the J/ψ p_T and rapidity have been weighted

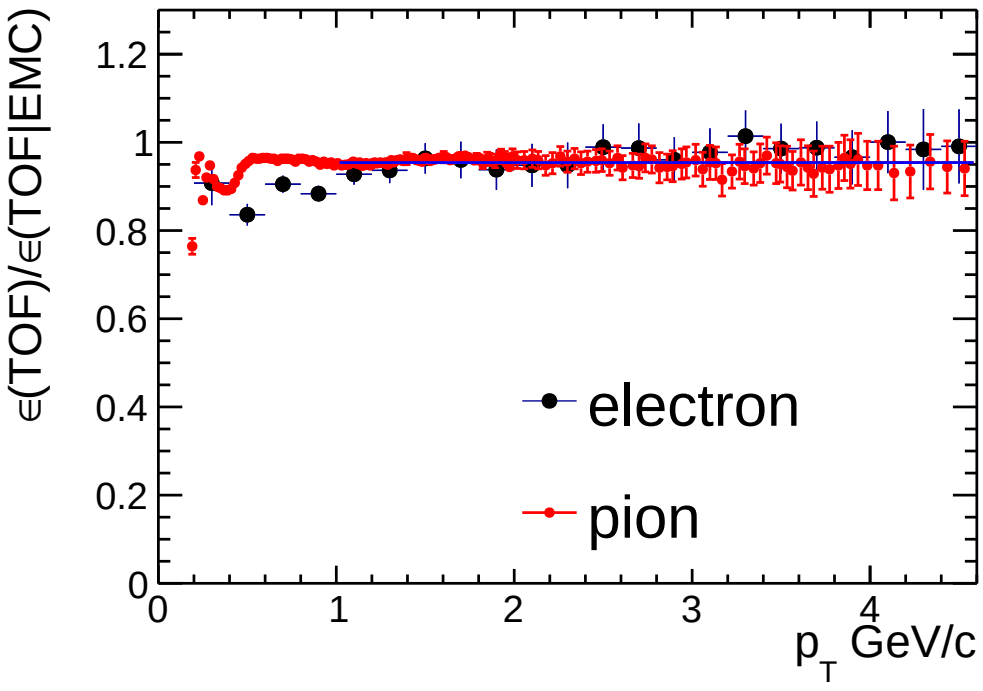

Figure 26: Ratio of TOF efficiency over TOF efficiency condition on no EMC matching for electron and pion in p+p MB at 200 GeV. Pion is taken from David's D* 2011AN.

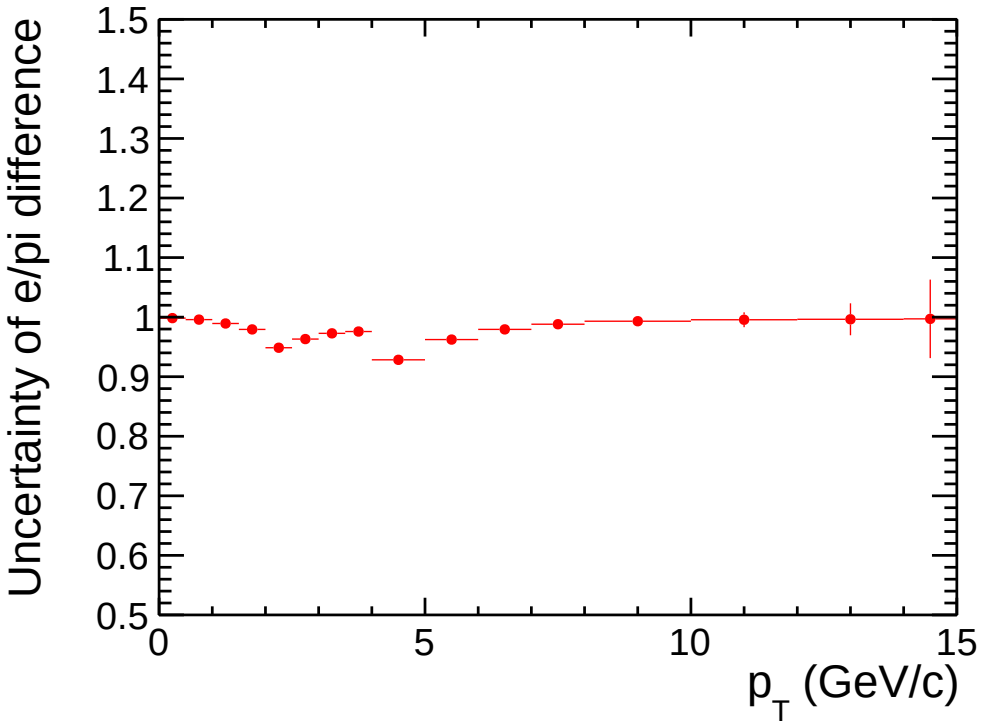

Figure 27: Uncertainty from difference between ratio r (P(TOF)/P(TOF—EMC)) from electrons and pions.

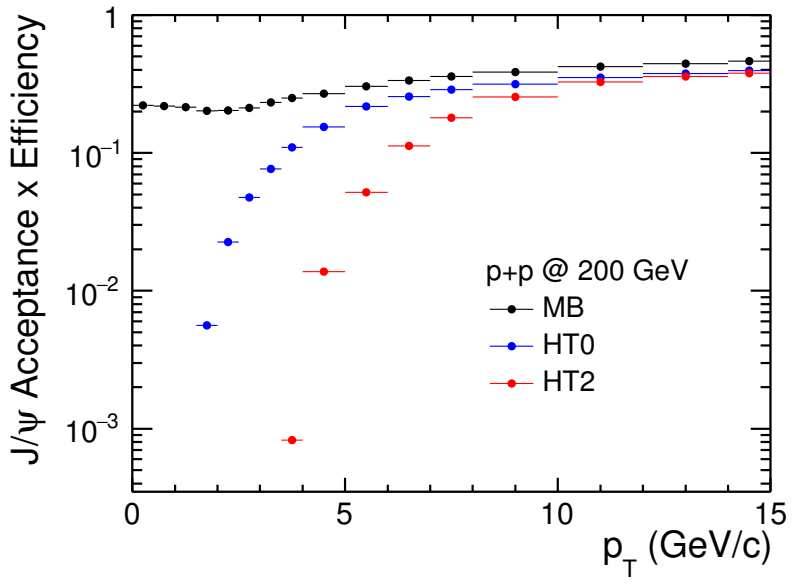

Figure 28: J/ψ overall efficiency in different triggers in p+p at 200 GeV, including TPC tracking, TOF matching, EMC, PID efficiencies, and acceptance.

to the Kaplan function $A(1+(p_T/B)^2)^{-6}$ with A = 4.23±0.12 and B = 4.10 ± 0.13 and a rapidity function $e^{-0.5y^2/1.416^2}$, which is obtained from previous J/ψ polarization analysis note SN0582. The uncertainties from these weights are fairly small, and are not taken into account.

Figure 28 shows the J/ψ efficiency in different triggers. Here the acceptance in Y-axis means the track loss outside of the detector acceptance, which is also taken into account in the embedding. Efficiency in HT triggers shows the J/ψ measurable p_T ranges. Even though HT0 has higher efficiency at 4 GeV/c, however, it has a prescale of 17 thus counts are less than HT2 at $p_T > 4$ GeV/c . J/ψ overall efficiency is calculated from folding each efficiency of single electron into the pair. We sampled all the efficiency of eID ($n\sigma_e$, $1/\beta$), TPC, TOF, EMC, and HT trigger for electrons from J/ψ decay in embedding, then applied same cuts as in data to reconstruct J/ψ , finally, the weighting factor of (p_T , y) of J/ψ production is applied to generated and reconstructed J/ψ . The overall efficiency is calculated from ratio of reconstructed J/ψ to generated one. The TPC, EMC, and HT trigger efficiency are simulated in embedding, therefore, related quantities (nHitsFit, energy, etc) are used directly in J/ψ reconstruction.

5.4 Trigger bias and efficiency

MB data have a trigger requirement of VPD coincidence on both east and west side. VPD is 5.7 m away from the center of TPC, the acceptance of VPD is $4.24 < |\eta| < 5.1$. Because of this limited acceptance, this trigger condition has a bias for J/ψ event, which may have more track in mid-rapidity than normal MB event. This bias factor was studied in D^0 and D^* analysis in Run9, which is around 0.67 for D^0 and 0.7 for D^0. However, there is a difference of vertex finding algorithm between Run9 and Run12. In Run12 p+p 200 GeV, high weight of TOF track is added into vertex finding algorithm, which is marked as " useBTOF4Vtx " option in production chain. This option significantly reduce the rate of pile-up events and bad events in reconstructed events. Also this option changes the bias factor caused by trigger.

The trigger efficiencies of VPDMB and BBCMB are simulated with the STAR detector Geant model, using PYTHIA8 as event generator. STAR default tune (PYTHIA8 tune 4C) is used for MB events, and HF tune is used for J/ψ events, the tunes are described in Sec. 3.

Two kinds of events, normal MB events and J/ψ events, are studied sepa-

rately. Figure 31 shows the numbers of events after different trigger and good vertex selections for these two kinds of events. "BBCAnd" and "VPDAnd" are corresponding to online BBCMB and VPDMB triggers, respectively. "Good Vertex" means the $|Vz_{Rc} - Vz_{Mc}| < 1.5cm$ in simulation. For MB events, the "Good Vertex && VPDAnd" efficiency is 21.7% in simulation. This efficiency for J/ψ events is 19.2%, which is shown in Fig. 32. No significant p_T dependence is found for this efficiency in J/ψ events. VPDMB trigger bias factor is 21.7/19.2 = 1.07, which is used in final results as PYTHIA8 is tuned for J/ψ analysis. The formula of trigger bias calculation is written as below:

$$f_{triggerbias} = \frac{N_{vpd\&GoodVz}/N_{all}}{S_{vpd\&GoodVz}/S_{all}} \tag{3}$$

where N is for number of events, and S is the number of signals.

Same study is done for PYTHIA6 as an event generator, with default STAR settings, the efficiency is 19.8% and 18.5% for the MB and J/ψ events, respectively. Then the VPDMB trigger bias factor is selected to be 1.13, and the difference (6%) to the result with correction factor 1.07 is taken as an uncertainty. From Fig. 31, the BBCMB trigger efficiency is 0.85 for MB events, and 0.81 for J/ψ events. This bias is also corrected for HT0 and HT2 events as they have BBCMB trigger condition. A cross check is also done by removing the useBTOF4Vtx option in reconstruction chain. This chain option allows the BTOF hits used in the vertex finding algorithm. Figure 33 shows the PYTHIA6+Geant result for J/ψ events without the chain option useBTOF4Vtx in pp200 in run12. The VPDAndGoodVtx efficiency for MB event is 16%. If we divided the efficiency of Jpsi event 22% in run9 simulation (from $D0$ AN), then we have a bias factor of 72%, which is close to the bias factor of D^0 in run9.

In p+p collisions, there are pile-up events can cause wrong vertex finding in event reconstruction. Although the collision rate is not high, we studied the pile-up effect on the trigger bias factor calculation. First we mix the PYTHIA event and zero-bias event together, then use the same vertex finding algorithm to reconstruct the vertex. We found the change of vertex finding efficiency is only 1%, a possible explanation is that the using of TOF track in vertex finding may reduce the false vertex probability. This difference is applied to J/ψ results in both MB and HT events. In VPDMB events, there is still a possibility that we reconstruct a vertex of pile-up event and it happens to be with 6 cm of Vz measure by VPD. We fit the $Vz_{TPC} - Vz_{VPD}$ distribution by two function Eq. 5, 6. The first function represents

the number of good vertices. The latter is the background, which is a random coincidence of a pile-up event and a real event. However, we don't know the true distribution of $Vz_{TPC} - Vz_{VPD}$. Thus another function Eq. 4 is used to estimate the uncertainty. The fit results are shown in Fig. 29. Left shows the Eq. 4 + Eq. 6, while Eq. 5 + Eq. 6 are shown in right. Another cross check is done by using Gaussian as background function, which shows worse performance of fit. The 3.7% correction from left panel is applied to VPDMB result. The difference between the left and right panel is used as the uncertainty of this source.

$$f_{s1} = p_0 e^{-(x-p_1)^2/(2p_2)} + p_3/(1 + (x/p_4)^{p_5}) \tag{4}$$

$$f_{s2} = p_0 e^{-(x-p_1)^2/(2p_2)} + p_3 e^{-(x-p_4)^2/(2p_5)} \tag{5}$$

$$f_{bg} = p_0 e^{-p_1|x-p_2|^{p_3}} \tag{6}$$

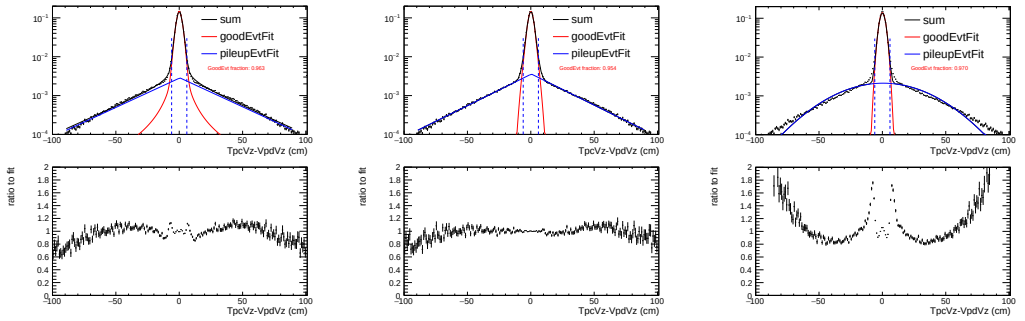

Figure 29: Fit of $Vz_{TPC} - Vz_{VPD}$ in VPDMB events. Left: Fit with Eq. 4 + Eq. 6 (background). Middle: Fit with Eq. 4 + Eq. 6 (background). Right: Fit with Eq. 5 + Gaussian as background

Since HT triggers are combined with BBCMB trigger, we have to evaluate the BBCMB trigger bias uncertainty. This uncertainty is estimated from the difference between results from PYTHIA6 and PYTHIA8, it is found to be 3%.

In addition to trigger bias correction, the numbers of equivalent MB events for HT0 and HT2 samples are calculated by comparing with MB

trigger after weighted their prescale factors in same run, which is

$$N_{eq}^{MB} = \frac{\sum_{|vz|<50} N_{HT}/\epsilon(vz)}{\sum_{allvz} N_{HT}/\epsilon(vz)} * (\sum N^{MB} * \frac{PS^{MB}}{PS^{HT}}) \quad (7)$$

where N_{HT} is used number of events from HT trigger, PS is the prescale factor. N^{MB} is the number of BBCMB events without any requirements. The summation covers all runs that have both BBCMB and HT triggers. $\epsilon(vz)$ is the HT trigger efficiency as a function of V_z. The HT sampled luminosity within $|Vz|$ <50 cm can not be determined by the HT V_z. distribution as the efficiency is not flat as a function of V_z.. Therefore, we have to correct the HT V_z to unbiased V_z distribution. In addition, the pile-up effect could reduce the vertex finding efficiency, and this effect may have V_z dependence. Therefore, we did a simulation to mix the PYTHIA event with zero-bias event as pile-up. The simulation is also described in previous paragraph. Figure 34 shows the V_z distribution and efficiency in BBCMB in the simulation. The V_z efficiency of BBCMB with ranking > 0 is nearly flat w.r.t true V_z. So we could use V_z in BBCMB with ranking > 0 to represent the true vertex Z distribution. The HT trigger efficiency is thus calculated by the ratio of HT V_z to BBCMB V_z, both have ranking > 0. Good vertex requirement with the ranking and $|Vz - Vz_{mc}|$ cut is only used for trigger bias study as we need to find out the bias for true events. One additional detail is that the V_z shapes of HT sample with and without ranking > 0 are very similar, the fraction of $|V_z| < 50$ cm is 65% without ranking cut versus 66% with ranking cut. We thus ignore the difference in the calculation of the equivalent number of MB events.

There is one more correction for BBC triggered events. The in-bunch pile-up is due to that multi-events are happening in same bunch. Therefore, since the BBC trigger rate in Run12 has a mean of 600 kHz, then the probability that we see a event in a bunch is 600 kHz / (9.38 MHz *102/120) = 0.075. This process satisfies Poisson distribution, thus we can calculate that probability of more than 1 events in BBC trigger is about 3.5 %. This 3.5% is increased in the equivalent number of MB events calculation. J/ψ decayed electrons have higher probability to fire the HT trigger. Therefore the vertex finding algorithm will preferably pick up the J/ψ vertex over the in-bunch MB vertex.

In the simulation, there is a small difference between the n_{ch} in PYTHIA and data Fig. 47. We use this difference as a weight in the simulation and

found the resulting trigger bias difference is 3% in BBCMB events and 5% in VPDMB events, These numbers are comparable or smaller than the uncertainty of PYTHIA generator, which is from the same source as the nch weighting. Therefore, the maximum value of the uncertainties from nch reweighting and PYTHIA tune is included in the final systematic uncertainty. Figure 35 shows the number of events after weight comparing with central values. Fig. 30 shows the efficiency changes with and without n_{ch} reweighting.

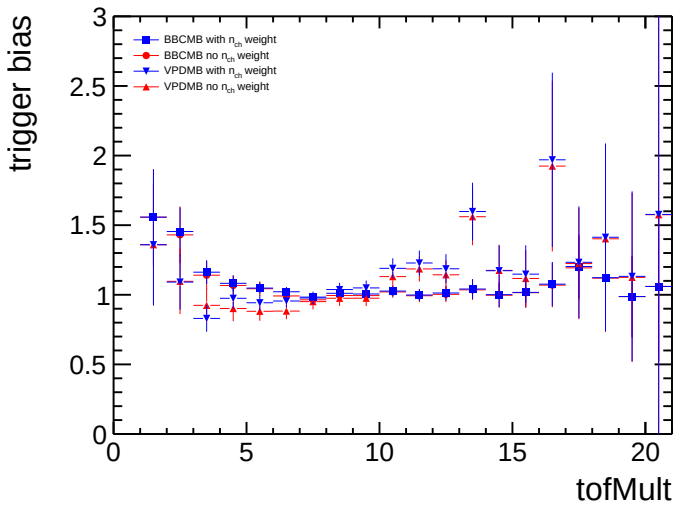

Figure 30: Trigger bias factors with and without N_{ch} weighted as a function of N_{ch} in J/ψ event in p+p at 200 GeV in PYTHIA+Geant simulation.

The full formula of calculating the J/ψ cross-section is as:

$$\sigma_{J/\psi} = \frac{\sigma_{MB}}{N^{eq}_{MB}\epsilon^{goodvtx}_{MB}} \frac{N^{raw}_{J/\psi}}{\epsilon^{HT}_{J/\psi}\epsilon^{trk}_{J/\psi}\epsilon^{eID}_{J/\psi}} \frac{\epsilon^{trg}_{MB}\epsilon^{goodvtx}_{MB}}{\epsilon^{trg}_{J/\psi}\epsilon^{goodvtx}_{J/\psi}} \tag{8}$$

, where ϵ^{trg}_{MB} is the trigger efficiency for MB events, and $\epsilon^{trg}_{J/\psi}$ is the trigger efficiency for J/ψ events. The last fraction is equivalent to the trigger bias correction factor, Eq. 5.4.

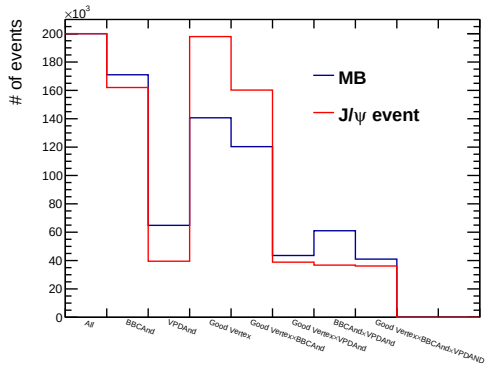

Figure 31: Number of events after different trigger and vertex selections in PYTHIA8+Geant simulation in p+p at 200 GeV.

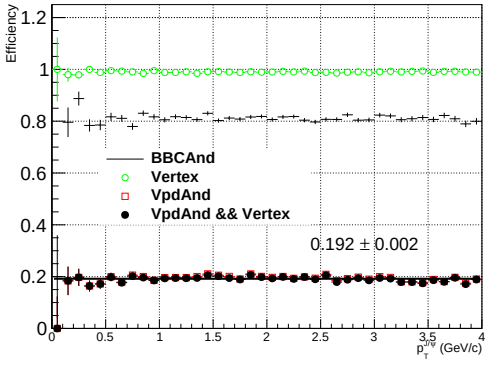

Figure 32: J/ψ efficiency in different combinations of triggers and good vertex requirement in PYTHIA8+Geant simulation in p+p at 200 GeV.

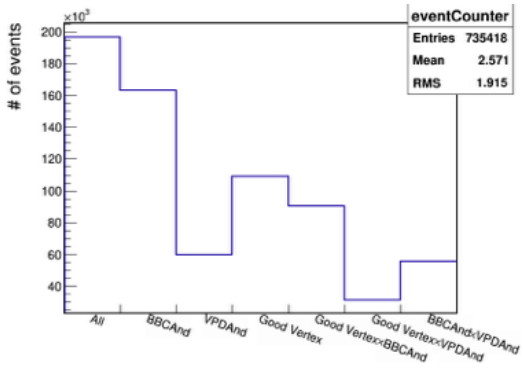

Figure 33: Number of MB events after different trigger and vertex selections in PYTHIA6+Geant simulation in p+p at 200 GeV without using BTOF hits in vertex finding algorithm.

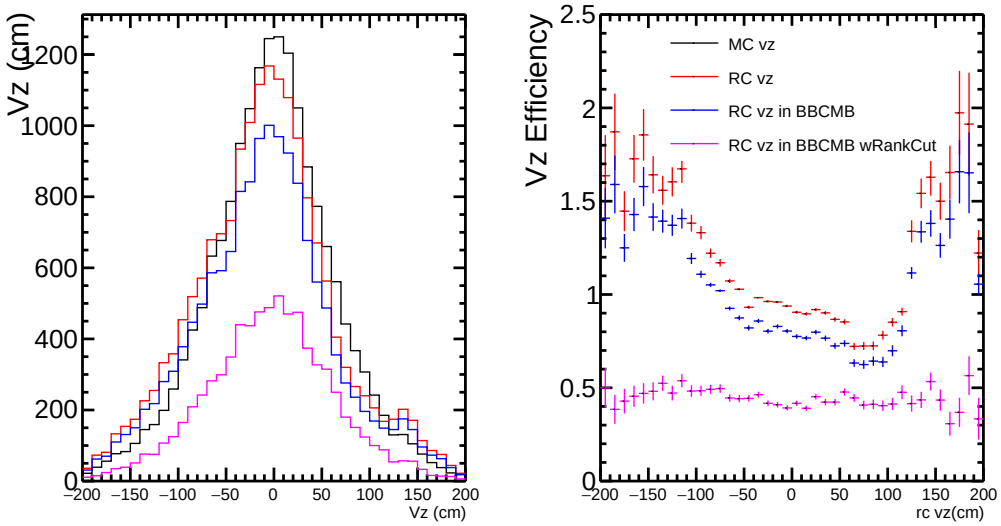

Figure 34: Vertex Z distribution and efficiency with pile-up in different requirements, BBCMB trigger with and without ranking > 0 cut .

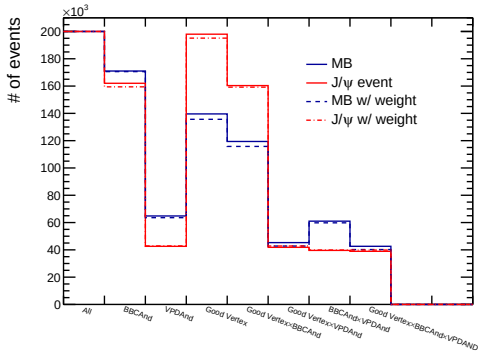

Figure 35: Number of MB events with n_{ch} weight in PYTHIA6+Geant simulation in p+p at 200 GeV.

6 Systematic uncertainty for J/ψ cross-section

The J/ψ cross-section systematic uncertainties are from the processes of fitting, efficiency calculations, and trigger bias correction. To estimate efficiency uncertainties, track cuts in both data and embedding are tuned at same time, and the J/ψ cross-section is recalculated for each tune. In total, there are 16 cut changes on nHitsFit, nHitsDedx, dca, nSigE, p/E, adc0, emc p_T lower limit, $1/\beta$. The uncertainty of the TOF matching efficiency is estimated by the fit 1-σ error. These changes are categorized into four types of TPC+TOF(nHitsFit +/- 2, nHitsDedx +2/-1, dca +/- 0.2, TOF matching 1σ), eID (nSigE +/- 1σ fit error, $1/\beta$ +/- 1σ), EMC (p/E +/- 0.1, emc p_T lower limit +/- 0.1), and trigger (adc0 +/- 16). Errors for each cut can be found in Table 7. Errors with same cuts are averaged, and then added in quadratic sum for each uncertainty category. The last two p_T bins have limited statistics, therefore, the uncertainties are from an extrapolation of previous p_T bins (2 to 10 GeV) by a constant function. The uncertainty of raw count extraction is not shown. It is estimated by changing fit mass range from default (2.5,3.8) to (2.7,3.6) GeV/c^2 and background shapes from linear to exponential distributions, which is about 7% on average. The VPDMB trigger bias uncertainty is calculated in last section, which is about 6% and only applied for $p_T <= 1.5$ GeV/c. BBC trigger bias uncertainty for HT0 and HT2 is estimated to be 3% by comparing results from different PYTHIA versions. The correlation between TOF and EMC efficiency is another source of uncertainty, it is about 1-7 %. All the uncertainties are shown in Tab. 7 and Fig. 36.

After all the corrections, the J/ψ cross-section from three triggers are shown in Fig. 37. In the overlap regions, the measurements are consistent with each other within errors.

The J/ψ p_T differential cross-section is shown in Fig. 38. It has been corrected for wide bin width effect. A levy function is fitted to the J/ψ p_T yield and then used to calculate the p_T position where the yield equals to the average of this wide bin. The detail method can be found in `http://www.star.bnl.gov/protected/lfspectra/marr/Analysis/PlaceDataPoints.pdf`. The Levy function describes the data quite well, the fit χ^2/ndf is 14/12. The final J/ψ cross-section from the sum of the data is $43.2 \pm 3.0(stat.) \pm 7.5(sys.)$, which is consistent with Run9 results.

Table 7: Systematic uncertainties of TPC+TOF, eID, EMC, HT trigger efficiency, TOF-EMC correlation correction and raw counts extraction as a function of p_T . Unit is percentage (%).

p_T	TPC+TOF	eID	EMC	trigger	effCor	raw	sum
0.25	10.5	7.32	9.41	0	0.165	14.3	21.4
0.75	4.2	4.72	5.46	0	0.415	3.25	8.97
1.25	4.92	4.41	8.51	0	1.07	14	17.7
1.75	5.93	4.72	8.55	3.54	2.06	9.26	15.3
2.25	12.5	11.5	13.7	8.22	5.14	3.56	24.1
2.75	10.6	9.8	9.13	6.33	3.68	7.01	19.9
3.25	16	13.5	13.6	11.4	2.72	2.73	27.7
3.75	11.8	11.2	7.7	7.12	2.42	7.45	20.9
4.5	11.3	9.52	11.3	5.19	7.17	1.24	20.6
5.5	12.8	9.58	9.46	6.33	3.77	3.35	20.3
6.5	12.1	12	9.69	6.87	2.06	6.04	21.7
7.5	13.4	9.16	9.76	6.32	1.19	4.25	20.4
9	10.8	10.7	11.7	4.37	0.685	6.17	20.6
11	12.4	10.8	10.7	6.91	3.2	7.4	22.3
13	12.4	10.8	10.7	6.91	3.2	7.71	22.4

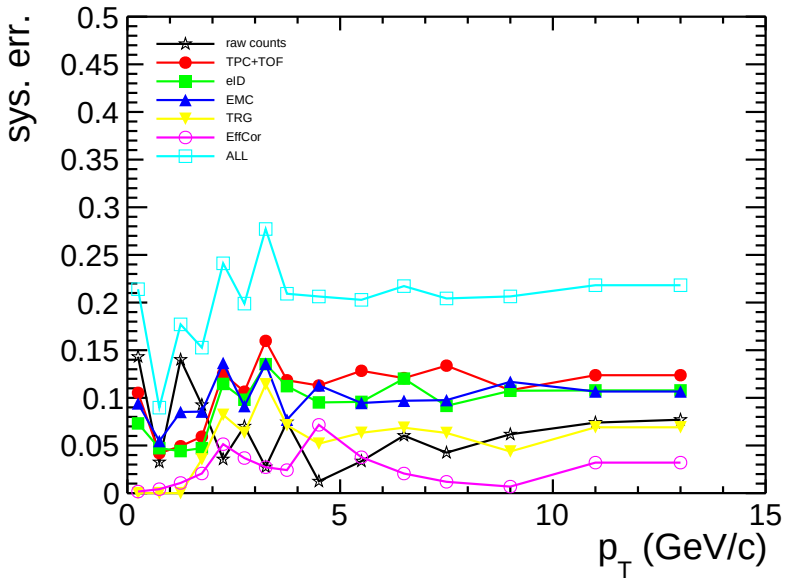

Figure 36: J/ψ systematic uncertainties of efficiencies in p+p at 200 GeV in Run12.

7 Event activity dependence of J/ψ production

J/ψ production mechanism is not yet fully understood in hadronic collisions. A substantial contribution of particles may be from Multi-Parton Interactions (MPI) in high energy p+p collisions. In PYTHIA, J/ψ production are expected to be independent of the overall event multiplicity. Recently, ALICE report J/ψ production is higher than PYTHIA in high multiplicity event, which indicates a substantial contribution of J/ψ may be from hard process of MPI in high energy p+p collisions. It's interesting to measure J/ψ production as a function of charge particle multiplicity in p+p at STAR.

7.1 Multiplicity of MB events

The charge particle multiplicity is measured using the tracks reconstructed in TPC and matched with TOF in BBCMB events. Track selections are listed in Tab. 8. TOF can significantly reject pile-up tracks and has a moderate

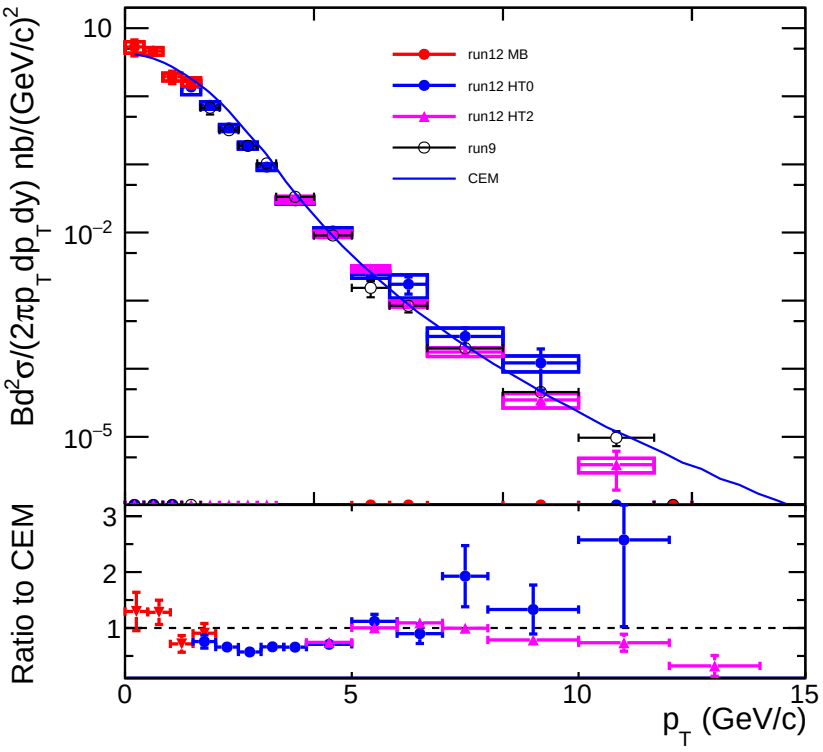

Figure 37: J/ψ cross-section from three triggers, VPDMB, HT0, and HT2, in p+p at 200 GeV in Run12.

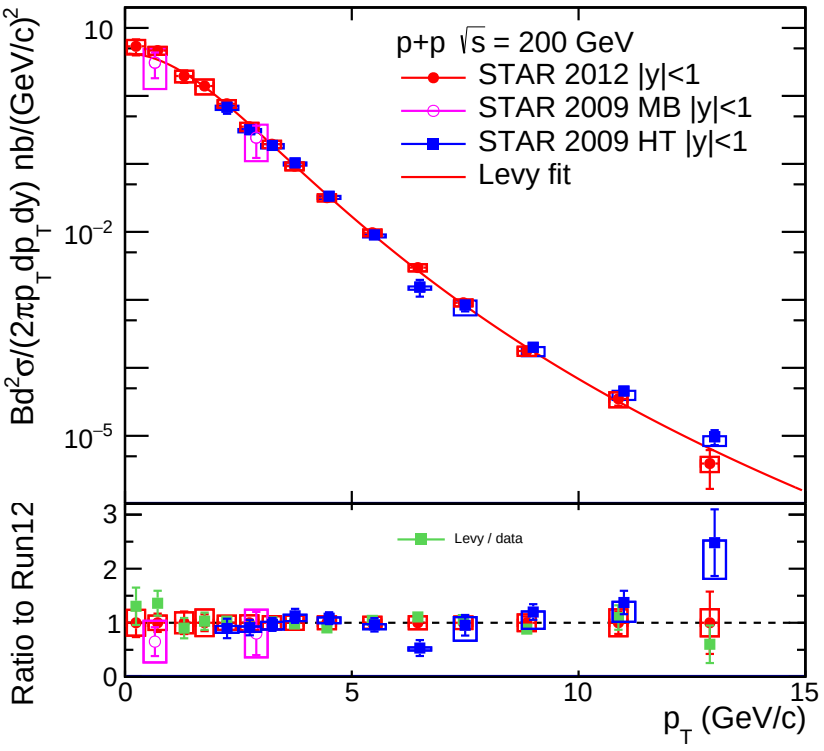

Figure 38: J/ψ p_T differential cross-section in p+p at 200 GeV in Run9 and Run12.

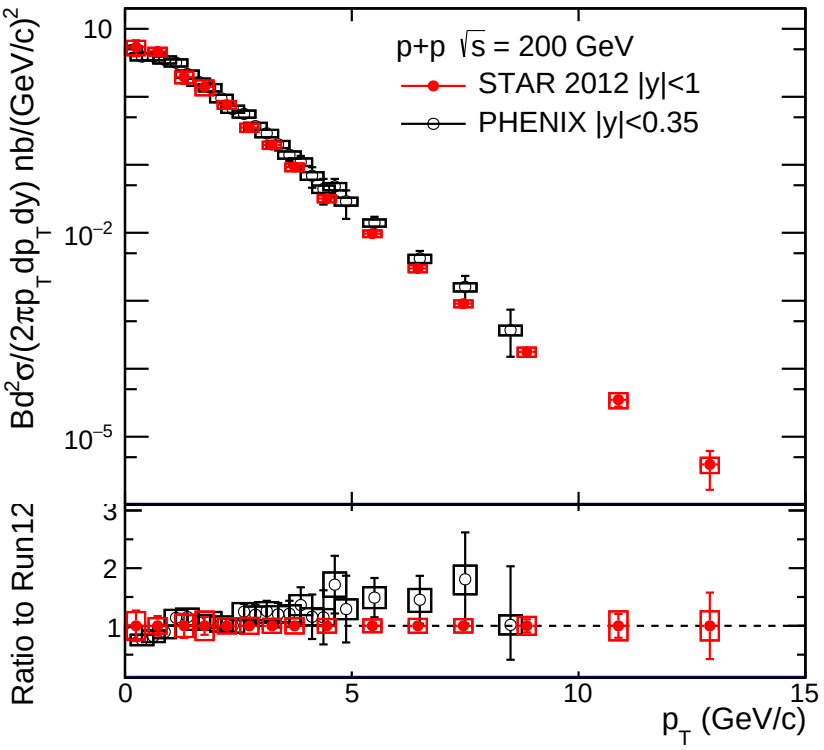

Figure 39: J/ψ p_T differential cross-section in p+p at 200 GeV in Run12 comparing with PHENIX result.

efficiency 60%., therefore, TOF multiplicity is chosen to calculate the event activity. Figure 41 shows the mean of TPC and TOF multiplicity within pseudo-rapidity (-1,1) before and after efficiency correction as a function of ZDC coincidence rate, which is proportional to luminosity. TOF multiplicity is near flat after efficiency correction while TPC increases as ZDC rate increases. Here charge particle efficiency is estimated from π, K, p TPC efficiency and TOF efficiency by weighting their yields. TPC and TOF efficiencies are estimated in embedding sample. The TPC efficiency calculation includes the p_T resolution effect by using RC p_T over MC p_T . Figure 42 shows the TPC and TOF efficiency as a function of ZDC rate. There is a decreasing trend for TPC efficiency as ZDC rate increases, however, TOF efficiency is nearly flat. The efficiency at higher ZDC bin has limited statistics, thus a linear function is used to fit the efficiency and to extrapolate to unmeasured range. Since the TOF efficiency is calculated from embedding, a comparison between TOF efficiency of charged particles in real data and embedding is shown in Fig. 40 to assure this method is valid.

In order to obtain corrected multiplicity (N_{ch}), an unfolding process is applied using RooUnfold package. The response matrix between true N_{ch} and raw N_{ch} (sampled TPC+TOF efficiency) is obtained from PYTHIA generator. The charged particles, π, K, p, e, and μ, are taken into account for N_{ch} in the simulation. The daughter tracks of K^0s, Λ are not included, and the tracks with starting vertex greater than 1 cm are excludes. All the tracks in N_{ch} calculation have $p_T > 0$ and $|\eta| < 1$. Two tunes (STAR default and Heavy Flavor tune) in PYTHIA8 are used in filling the response matrix. HF tune is used for central value, and STAR default is for uncertainty study.

The raw N_{ch} in simulation is defined as the number of charged particles have $p_T > 0.2$ GeV/c , $|\eta| < 1$, and $dca < 1$ cm. The track in raw N_{ch} is selected by a random generator with range of (0, 1), if the random number less than the TPC and TOF efficiency then this track is accepted in raw N_{ch} calculation. In J/ψ event, there is an addition requirement that the event is required to have two J/ψ decayed electrons within $|\eta| < 1$. The response matrix is filled with raw N_{ch} and true N_{ch}.

The response matrix is used to fold raw N_{ch} from data to real distribution. Before this process, the vertex finding efficiency and BBCMB trigger efficiencies are corrected for the raw N_{ch} in data. These efficiency are studied with PYTHIA8+Geant simulation with HF tune. The requirements for good vertex are $|vz| < 50\ cm$ and $|vz - vzMc| < 3\ cm$ in simulation. The BBCMB coincidence is reproduced by Geant simulation. The uncertainties of these

efficiencies are studied via different PYTHIA versions (8 and 6). Figure 43 shows these two efficiencies. It is only used to correct MB raw data. Figure 44 shows the efficiencies used for J/ψ data sample. With these two corrections, the raw TOF N_{ch} is unfolded by the RooUnfoldBayes method with the response matrix from PYTHIA. Figure 47 shows the raw N_{ch} and corrected N_{ch} in data and PYTHIA. A negative-binomial distribution (NBD) function is fit to the data. It shows a good consistency between the data and NBD. The fit is also shown in Fig. 48 including the systematic uncertainty and the ratio of data to fit. The uncertainties of N_{ch} caused by tracking efficiency, vertex finding efficiency, and PYTHIA unfolding are listed in Tab. 9. Final result is 2.87 $\pm$ 0.27 (stat.) $\pm$ 0.25 (model.) $\pm$ 0.41 (syst.), the second error is for the difference between direct mean and NBD fit result.

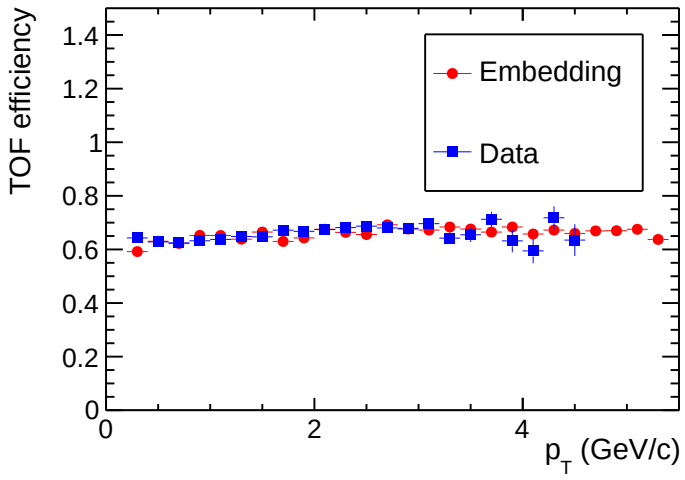

Figure 40: TOF efficiency comparison between data and embedding in p+p at 200 GeV.

7.2 Multiplicity of J/ψ events

The number of J/ψ event as a function of raw TOF N_{ch} is calculated subtracting like-sign from unlike-sign ee pair as a function of raw TOF N_{ch}. The residual background is studied in several wide n_{ch} bins, it is found that has no obvious n_{ch} dependence, which is shown in Fig. 50. Therefore, the residual background can be canceled out in final calculations. Only a p_T de-

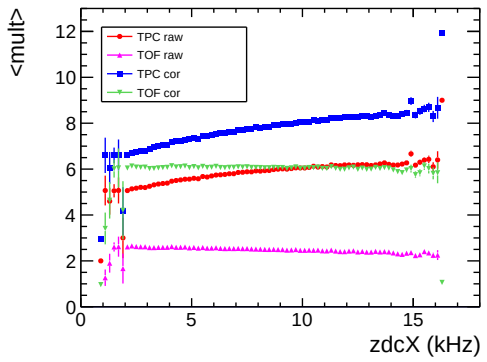

Figure 41: Mean of TPC and TOF track multiplicity in $|\eta| < 1$ before and after efficiency correction as a function of ZDC coinicidence rate in p+p at 200 GeV in Run12.

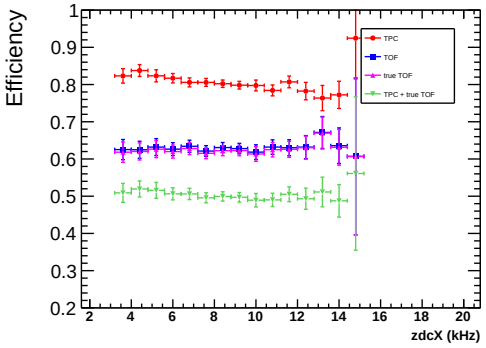

Figure 42: TPC and TOF efficiencies of pion in p+p at 200 GeV.

Table 8: Charge particle track quality cuts used for TOF multiplicity calculation.

$0.2 < p_T < 50$ GeV/c
$-1 < \eta < 1$
$dca < 1$ cm
$nHitsFit >= 15$
$nHitsRatio > 0.52$
tofMatchFlag > 0
$\|yLocal < 2$ cm

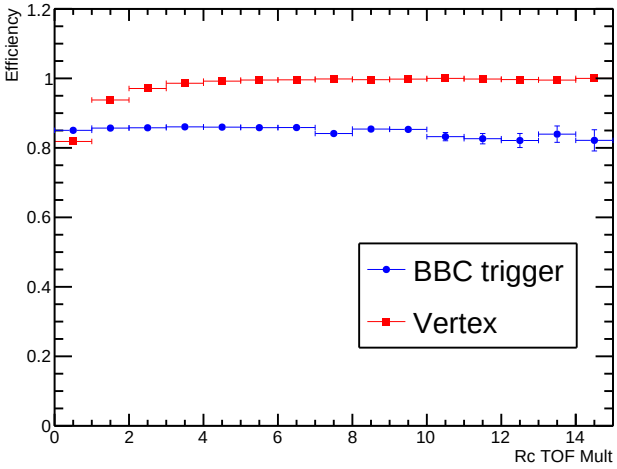

Figure 43: BBC trigger efficiency and Vertex finding efficiency as a function of raw N_{ch} in MB p+p at 200 GeV in PYTHIA+Geant simulation.

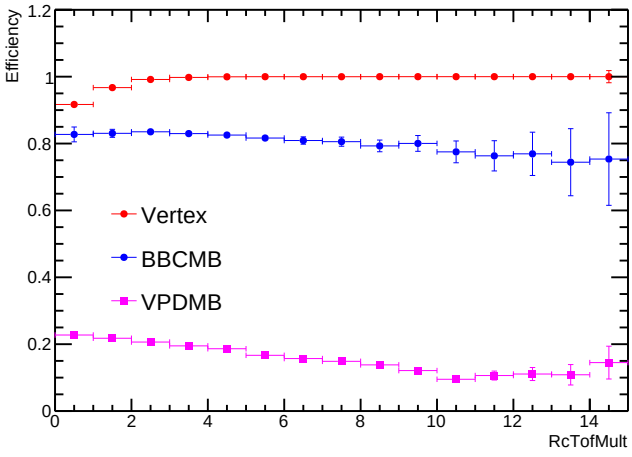

Figure 44: Vertex finding efficiency as a function of raw N_{ch} in J/ψ event in p+p at 200 GeV in PYTHIA+Geant simulation.

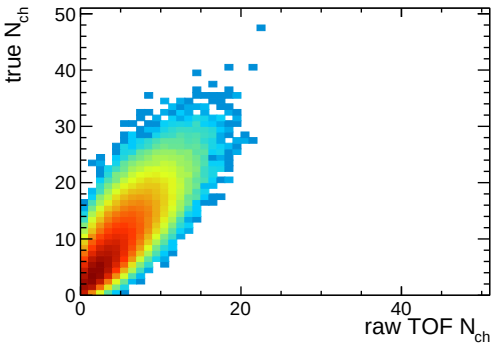

Figure 45: Response matrix of n_{ch} and raw TOF n_{ch} in MB p+p at 200 GeV in the PYTHIA.

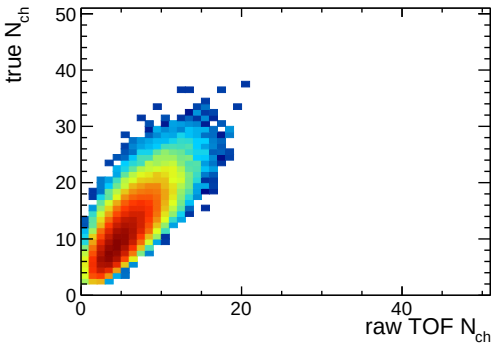

Figure 46: Response matrix of n_{ch} and raw TOF n_{ch} in J/ψ events in p+p at 200 GeV in the PYTHIA.

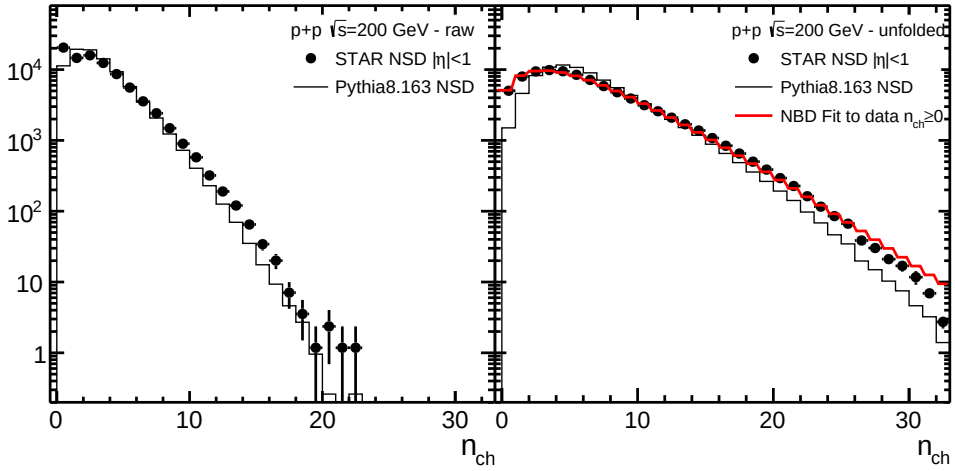

Figure 47: Raw (left) and corrected (right) N_{ch} in p+p at 200 GeV in the data and PYTHIA.

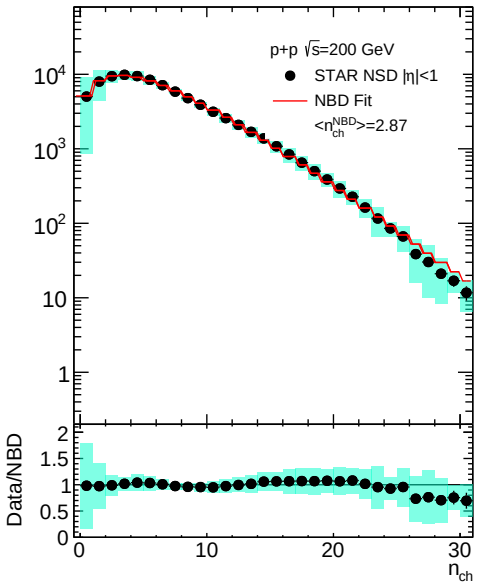

Figure 48: Corrected N_{ch} in p+p at 200 GeV in the data with NBD fit.

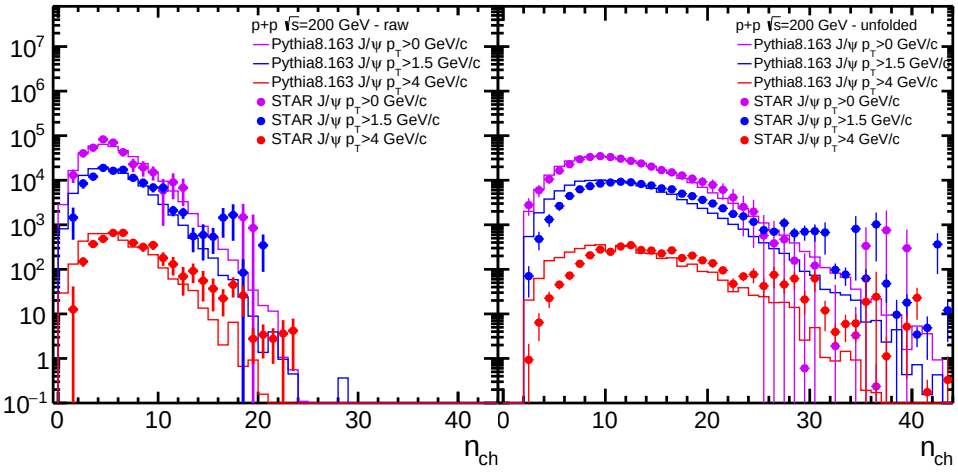

Figure 49: Raw (left) and corrected (right) N_{ch} of J/ψ events in p+p at 200 GeV in the data and PYTHIA.

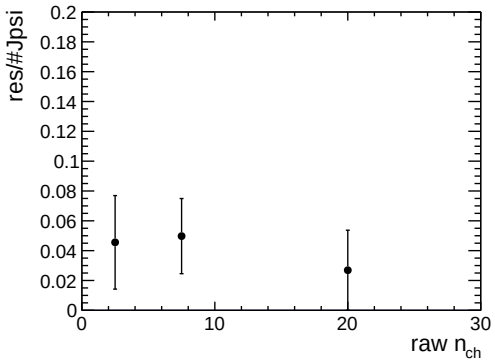

Figure 50: Residual background vs the number of J/ψ counts as a function of n_{ch}.

pendent pair efficiency is considered for J/ψ raw multiplicity distributions. This efficiency is calculated in the same way of Sec. 5.3, and is applied to each raw TOF N_{ch} bin. Figure 45 and Fig. 46 show the response matrices of N_{ch} and raw TOF N_{ch} in MB and J/ψ events, respectively .

The unfolding process of J/ψ event multiplicity is same as MB events. The multiplicity of J/ψ event in PYTHIA has conditions of including two electrons from J/ψ , $|\eta_{J/\psi\to e}| < 1$, $p_T > 0$, no tracks from K^0s and Λ, and no tracks with distance to starting vertex greater than 1 cm. Only those Jpsi events in which decayed electrons pass PID requirements are used to generate the response matrix.

Two different unfolding methods, Bayesian and SVD, are used, the difference between two methods is taken into account of uncertainty. The Bayesian method is the default method. The Bayesian and SVD methods both have a parameter need to choose. It is the number of iterations in Bayesian method, and the regularization parameter (kReg) in SVD method. Fig. 51 and Fig. 52 show the χ^2 as a function of the parameters (nIterations and kReg) in two methods. These parameters are chosen as nIter = 3, and kReg = 4 by default. We also vary nIter to estimate the uncertainty of the Bayesian method.

For three triggers, VPDMB, HT0, and HT2, different p_T cuts used to fill the response matrices. Figure 49 shows the raw and corrected multiplicity distribution of J/ψ events.

Both MB and J/ψ event multiplicity distributions are obtained from above studies. The unfolded n_{ch} distributions are shown in Fig. 53. The statistical errors are high correlated shown as Fig. 54. The error of merged

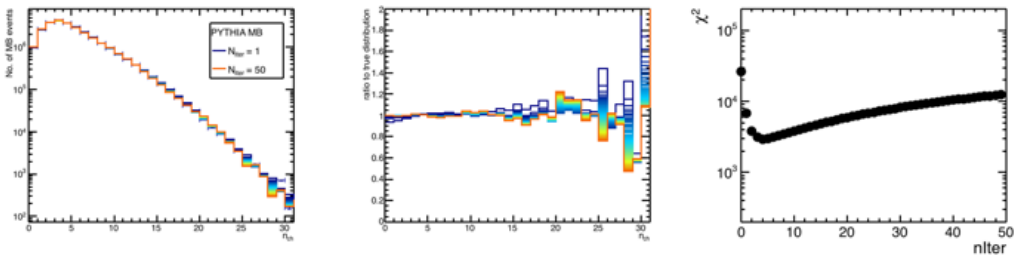

Figure 51: n_{ch} distrbutions (left), ratios of unfolded to true n_{ch} distributions, and χ^2 vs the number of iterations (right) in Bayesian unfolding method in PYTHIA MB events.

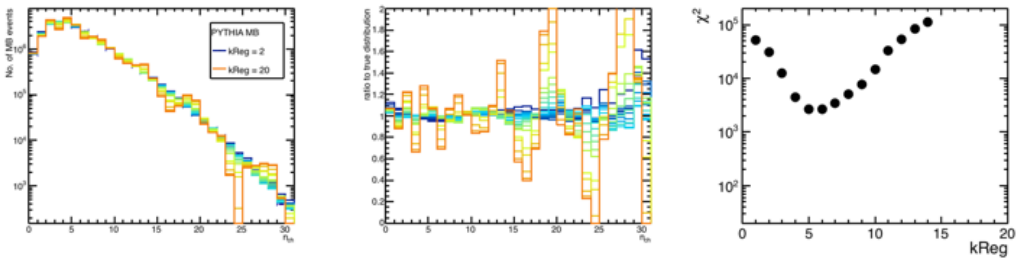

Figure 52: n_{ch} distrbutions (left), ratios of unfolded to true n_{ch} distributions, and χ^2 vs the regularization parameter in SVD unfolding method in PYTHIA MB events.

n_{ch} is calculated by the covariance matrix.

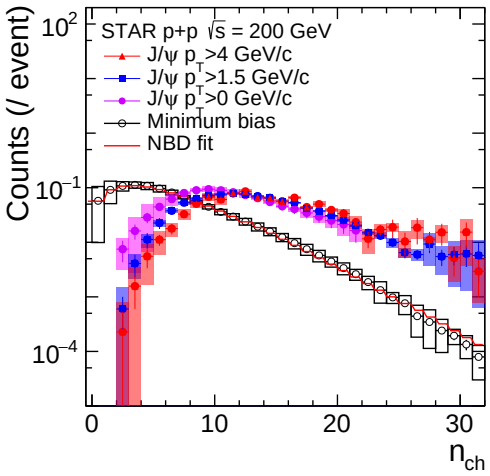

Figure 53: Unfolded n_{ch} distributions of MB, J/ψ MB, HT0, and HT2 events.

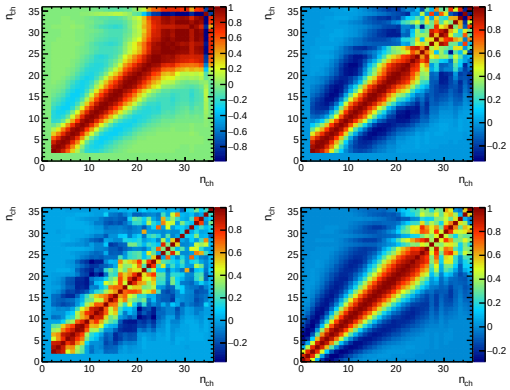

Figure 54: Correlation coefficient matrix of n_{ch} in J/psi MB (top left), HT0 (top right), HT2 (bottom left), and MB (bottom right) events.

The $N_{J/\psi}/ < N_{J/\psi} >$ vs $TOFMult/ < TOFMult >$ can be easily calculated with these distributions. The n_{ch} distribution is split into six bins: 0-5, 6-10, 11-15, 16-21, 22-31. Figure 61 shows the results for three triggers. The last bin of MB trigger is removed due to the large statistical error.

8 Systematic uncertainty for J/ψ event activities.

The systematic uncertainties are from vertex finding efficiency, tracking, unfolding process, and pile-up estimation. Vertex finding efficiency uncertainty is studied with different version of PYTHIA as mentioned previously. PYTHIA generator has 6% dN/dy difference of pion, kaon, proton yields comparing with data. The number of produce charged particles are tuned by ± 6%, and difference in final results are propagated to final systematic uncertainty. This uncertainty includes the tracking uncertainty, because the major uncertainty of particle yield is from the tracking. So it is categorized

in tracking uncertainty. The unfolding process uncertainty is estimated by varying the unfolding methods from Bayesian to SVD, the used number of iterations (from default 3 to 5) used in Bayesian, and the response matrices calculated from PYTHIA events with two different settings. The uncertainty caused by pile-up events is estimated from the difference between data and NBD fit and the difference from two ZDC efficiency corrections of ZDC rate 1-3 and 11-13 kHz. The default value is from ZDC rate 1-3 kHz. Figure. 55 shows the difference.

The trigger bias uncertainty for n_{ch} has been studied with PYTHIA + Geant, which is shown as "n_{ch} weighted" in Fig. 56. We obtained the trigger and vertex finding efficiencies as a function of TofMult by weighting the PYTHIA events with unfolded n_{ch} distribution from data, and then calculated the multiplicity distributions in MB and J/ψ events again. The differences between the trigger and vertex efficiency with and without n_{ch} weighting in J/ψ events are shown in Fig. 57. Since the uncertainty from n_{ch} reweighting is similar as PYTHIA tune, which is related to the change of n_{ch} distribution, the maximum value of these two sources is added into final systematic uncertainties.

Figure 59 shows the systematic uncertainties of n_{ch} in MB events.

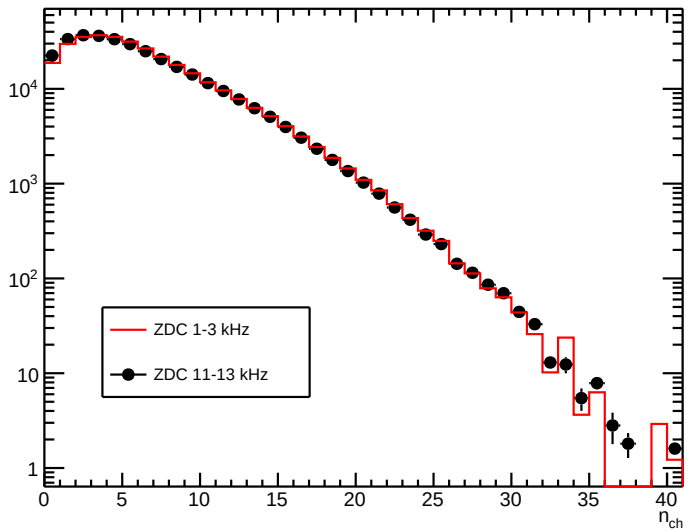

Figure 55: Unfolded n_{ch} distributions in different ZDC rates.

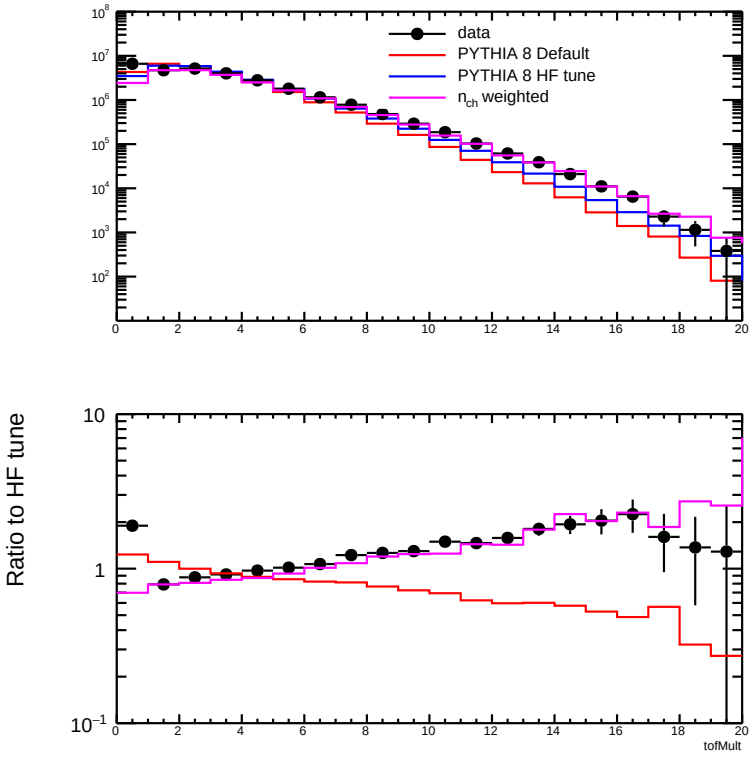

Figure 56: Raw n_{ch} distributions in different versions compare with data.

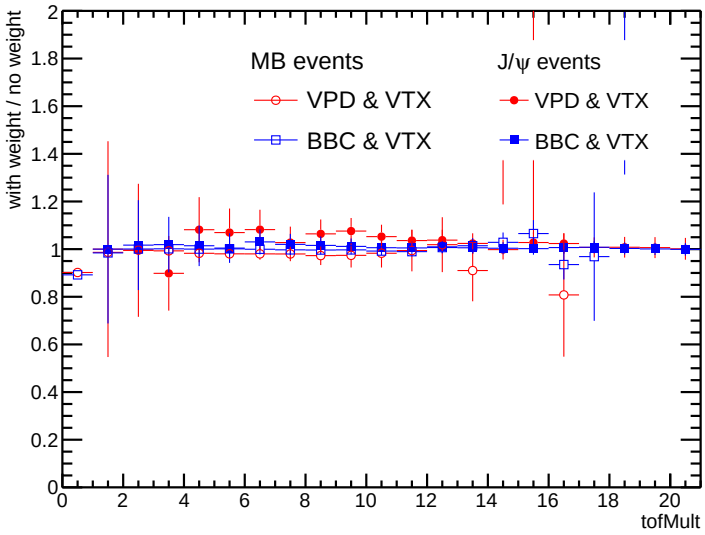

Figure 57: Trigger and vertex efficiency as a function of raw n_{ch} with and without n_{ch} weight in J/ψ events.

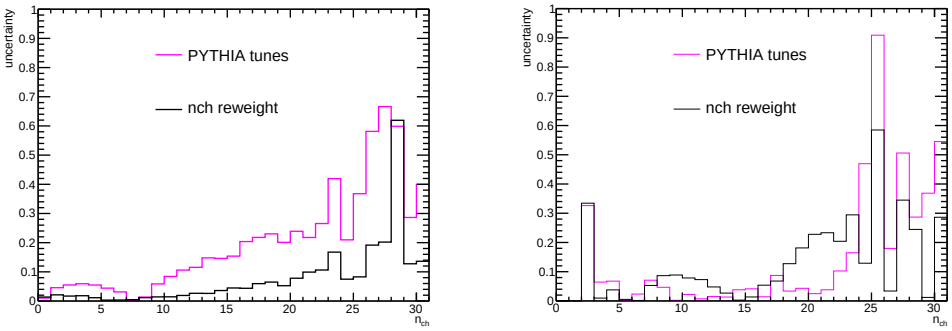

Figure 58: Differences from n_{ch} reweight and PYTHIA tunes in MB (left) and J/ψ (right) events.

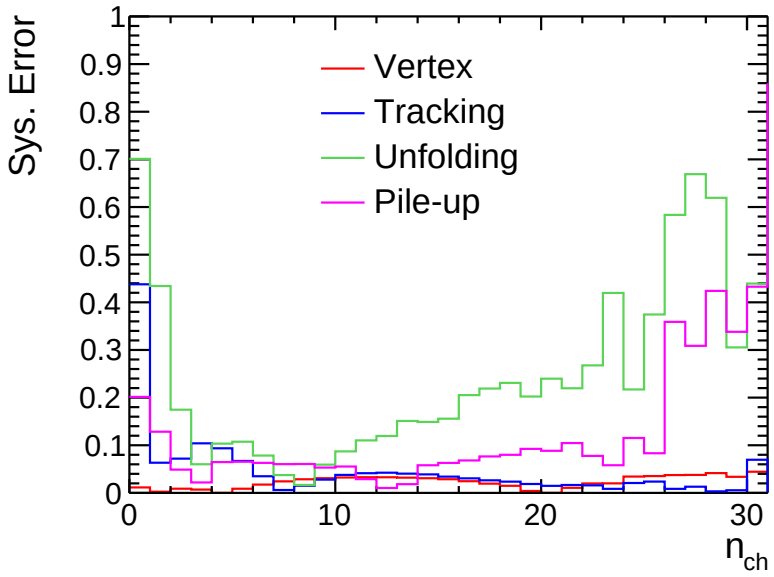

Figure 59: n_{ch} systematic uncertainties of MB events.

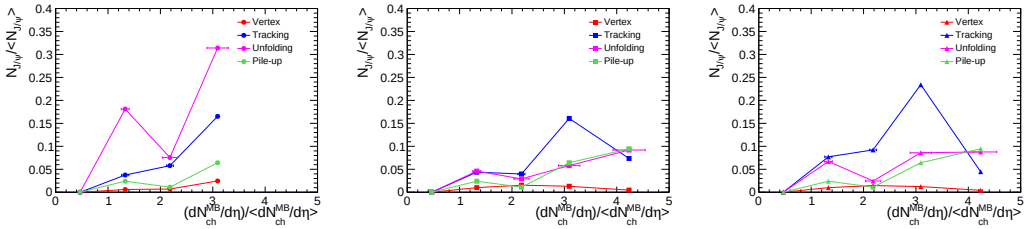

Figure 60: Systematic uncertainties in J/ψ MB (left), HT0 (middle), and HT2 (right) samples.

Figure 60 show the uncertainties from Vertex finding, tracking, unfolding, and pile-up in three J/ψ data samples, MB, HT0, and HT2.

Figure 61 shows the result with systematic uncertainties. Table 9, 10 summarize all the systematic uncertainties.

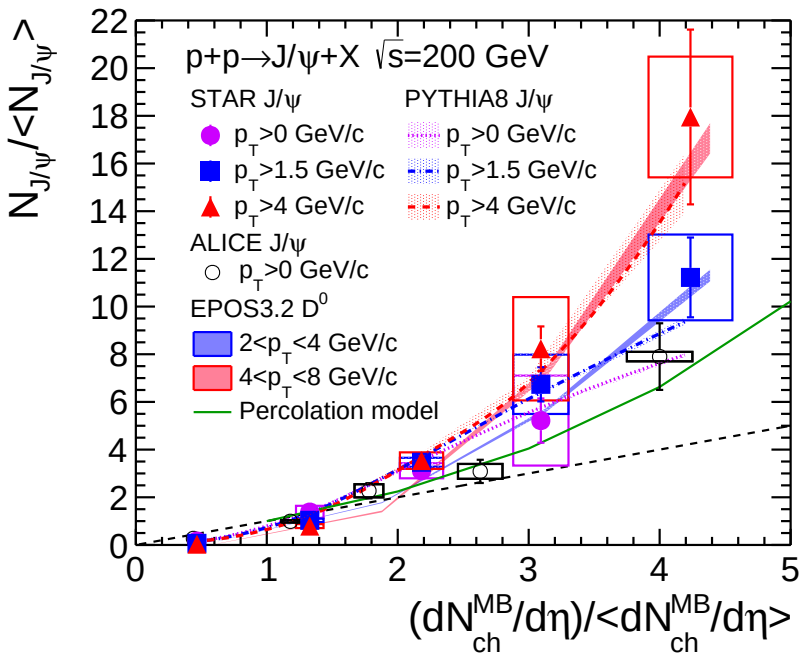

Figure 61: J/ψ production as a function of event activity in p+p at 200 GeV. Boxes show the systematic uncertainties

Table 9: Systematic uncertainties for the MB event $< n_{ch} >$ measurement

Vertex finding	2
Tracking	5
Unfolding	13
Pile-up	2
Total	14.2

Table 10: Systematic uncertainties for the J/ψ event activity measurement.

Type	Uncertainty (%)	
	$\frac{dN_{ch}^{MB}/d\eta}{<dN_{ch}^{MB}/d\eta>}$	$\frac{N_{J/\psi}}{<N_{J/\psi>}}$
Vertex finding	2	2-3
Tracking	4-5	4-23
Unfolding	2-7	1-30
Pile-up	2	1-10